Aspects of Black holes and jets

A. Mangalam[†]

[†] IIA, Bangalore

Extragalactic relativistic jets: cause and effect, ICTS
13 October, 2015

Outline

- Observational aspects of black holes
- $M - \sigma$ relation
- Tidal Disruption Events
- Non-relativistic jet theory
- Self consistent jet models

Observational Signatures of MDO, SMBH

Observations: A Jigsaw Puzzle

- $M_\bullet$ from stellar orbits (Kormendy 1995, 2009)
- Variability gives $\tau \sim r/c$, Doppler width $< v >^2 \sim GM/R$; Peterson & Wandel 2002

  Masing: Keplerian Curve $\Rightarrow$ Spherical distribution; Miyoshi et al 1995, Ford 94
- Relativistic Jets suggest compactness.
- $L - z$, $n(z)$. SDSS suggests Quasar distribution peaks $z = 2 - 3$
- $M_\bullet \propto \sigma^\gamma, \quad \gamma = 4 - 5$; $M_\bullet \propto M_{\rm bulge}$
- X-ray/UV flashes around MDOs
- GRBs: Black hole related?

Complicated set of clues, issues are inter-linked.

Basis for theoretical modelling

No hair theorem: $M_\bullet, J, Q$; $Q = 0$. Wheeler, Carter (1979)

Available schemes:

- Gas dynamical: $M_\bullet, \dot{M}, \dot{J}, L, L_j$

  Can be further classified into Hydro, MHD, Radiation- Hydro, Radiation-MHD, GRMHD.

- Electrodynamical: $M_\bullet, B, j, L_j$

- Stellar dynamical: $M_\bullet, \dot{M}, \dot{J}, L, n_c \propto r^\alpha, r_c, L_x \propto T^{-5/3}$

Schemes are complicated, but need to inter-link them as observables are inextricably entwined.

Determination of black hole mass in AGN

- These include direct astrometric measurements tracing the highly elliptical orbit of a star close to the compact core in Sagittarius A* indicate a Keplerian orbital period of 15.2 years and a pericentric distance of $\sim$ 17 light hours with the best fit to the observations requiring a mass of $\sim 10^6$ $M_\odot$ (Schodel et al 2002).
- Gas dynamics based tests
- Stellar dynamical tests
- Studies on water maser emission
- Reverberation mapping
- Searches for quasi-periodic signals.

Water maser emission

H2O maser emission at λ = 1.35 cm ($\sim$ 22 GHz) can be used to trace single gas clouds orbiting massive black holes in galactic nuclei.

$$v_{\rm obs} = \left(\frac{G\,M_{BH}}{s}\right)^{1/2} \sin i. \qquad (1)$$

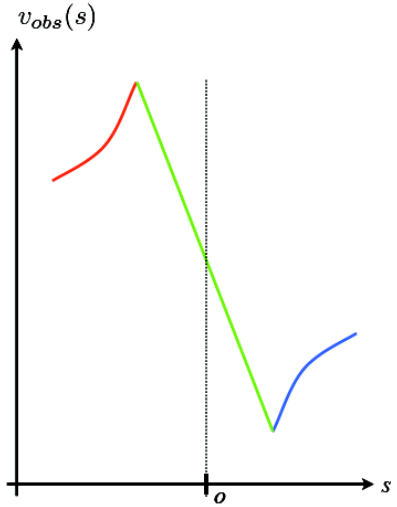

Figure: The rotation curve showing the velocity of a water maser emission source. The disk, likely to be the outer portion or an extension of an accretion disk is gravitationally bound to the central black hole. Image courtesy: Alessandro Marconi.

Gas and stellar dynamics based measurements

- The dynamical motion of gas and stars in the nuclear region of a galaxy are studied in a statistical manner to derive their average velocity v from the velocity distribution and the dispersion σ in the velocity.
- As an estimate of σ for the gas is available in many cases and the relationship between σ and r is known
- Hubble Space Telescope (HST) studies on M 87, a giant elliptical galaxy indicate a SMBH mass of $\sim 2.4 \pm 0.7 \times 10^9$ $M_\odot$ from narrowband Hα imaging (Ford et al. 1994) and O [III] 4959 Å line (Harms et al. 1994) and $3.2 \pm 0.9 \times 10^9$ $M_\odot$ from the O [II] 3727 Å line (Macchetto et al 1997).
- A similar HST narrowband Hα imaging study on NGC 6251 indicates a SMBH mass of $4 - 8 \times 10^8$ $M_\odot$ (Ferrarese & Ford 1999) and HST based spectroscopic study in the S [III] 9533 Å line of Centaurus A indicates a SMBH mass of $\sim 10^8$ $M_\odot$ (Marconi et al. 2006)

Reverberation mapping and virial estimation

For a virialized gas cloud,

$$M = frv^2/G$$

where f is a covering fraction which must be used to account for the shape of the BLR clouds and other geometrical effects, The expression for the virial mass thus contains three parameters f, r and v^2 which must be constrained from observational studies.
The time delay $\Delta\tau$ between continuum and line variations are used to place upper limits on r as $r = c\Delta\tau$. The measurement of these time delays can thus be used to determine the r.
Also r can be determined through a virial relationship between the broad line region radius for the Hβ or C[IV] emission line and the bolometric luminosity. $r \propto L^{0.6\pm0.1}$. The line width from multiple emission lines are used to measure v^2 by considering the full width at half maximum.
An estimation of f is generally carried out by comparing the estimated M/f with the black hole mass obtained from the $M - \sigma$ relation. It is found that f is typically constrained to $\sim$ 0.75 to 1. Thus, M_{BH} can then be determined.

Determination of black hole spin in AGN

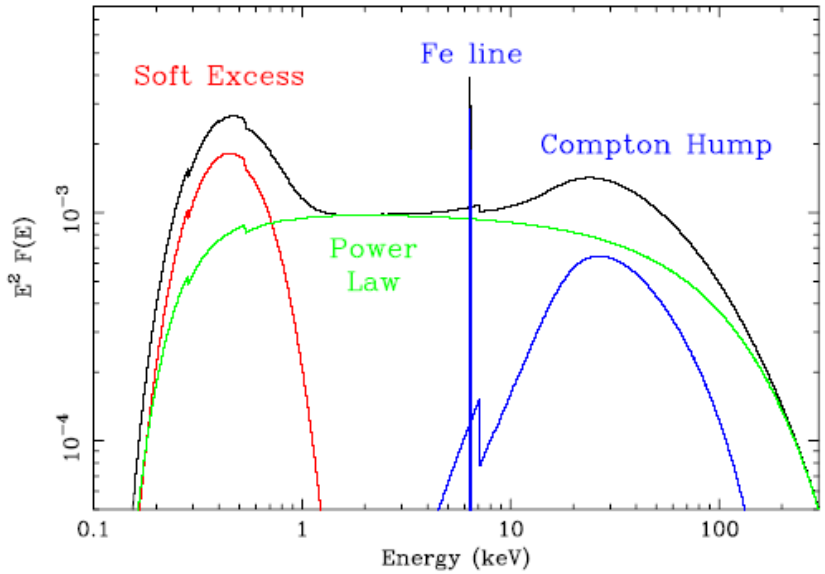

Figure: The main components of the X-ray spectra of unobscured accreting BH are shown: soft X-ray emission from the accretion disc (red); power law from Comptonization of the soft X-rays in a corona above the disc (green); reflection continuum and narrow Fe line due to reflection of the hard X-ray emission from dense gas (blue). Image courtesy: Fabian 2006.

Determination of black hole spin in AGN

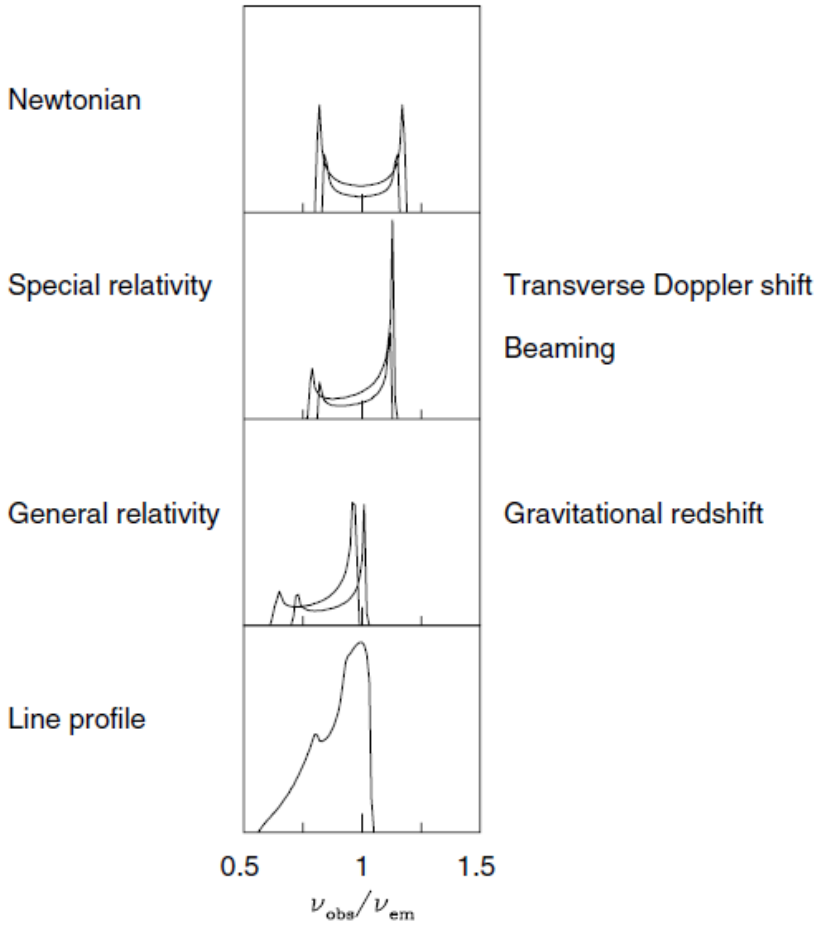

Figure: An intrinsically narrow emission line is modified by the interplay of Doppler/gravitational energy shifts, relativistic beaming, and gravitational light bending occurring in the accretion disc (from Fabian et al. 2000)

Determination of black hole spin in AGN

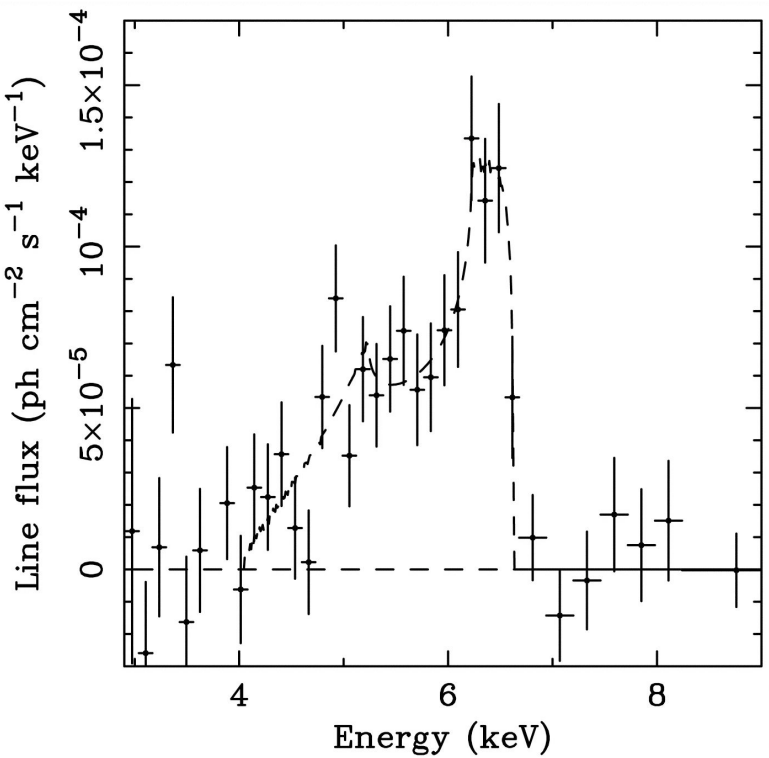

Figure: The line profile of iron K emission in the ASCA SIS spectrum of the Seyfert 1 galaxy MCG-6-30-15. The line shape is skewed toward energies lower than the rest energy of the emission line (6.35 keV at the source with z = 0.008). The dotted line shows the bestâfit line profile from the model of Fabian et al. 1989. Image Courtesy: Tanaka 1995.

Introduction to $M_\bullet - \sigma$ relation

- All massive galaxies have a supermassive black hole (SBH) at their centers.
- At distances close to the center of these galaxies stellar motions are completely dominated by the gravitational force of the SBH, but at further distances from the center the motion is influenced by other nearby stars.
- There is a strong correlation between the mass of SBH and velocity dispersion σ of the stars in the galaxy.
- The relationship of mass of stellar spheroids and their luminosity goes as $M_{Bulge} \sim L^{\frac{5}{4}}$.

- Faber - Jackson law for elliptical galaxies:
  $\log_{10}\left(\frac{\sigma_{||}}{150 kms^{-1}}\right) \simeq 0.25 log_{10}\left(\frac{L_R}{10^{10} h_7^{-2} L_\odot}\right)$.
- Therefore, $L \sim \sigma^4$ which in turn implies that $M_{Bulge} \propto \sigma^5$.
- There is a fixed ratio of SBH mass to the bulge mass of galaxies.
- Since there is a proportionality relation between M_{Bulge} and $M_\bullet$, it can be written as $M_\bullet \propto \sigma^5$.

Significance of the $M_\bullet - \sigma$ relation

- Energy driven Flow : SBHs acquired most of their energy via accretion of gas (Soltan., 1982).
- SBHs eventually reach a saturated mass when further accretion is prevented because of outflow.
- The ratio of energy released to the gravitational binding energy of the bulge is:

$$\frac{\eta M_\bullet c^2}{\frac{GM_{Bulge}^2}{R_{Bulge}}} \approx \eta \frac{M_\bullet}{M_{Bulge}} \frac{c^2}{\sigma^2}$$

$$\approx 225 \left(\frac{\eta}{0.1}\right) \left(\frac{\frac{M_\bullet}{M_{Bulge}}}{10^{-3}}\right) \left(\frac{\sigma}{200 kms^{-1}}\right)^{-2} >> 1$$

- Therefore, in the formation of SBH more than enough energy is released to unbind the total mass of a galactic bulge.

Significance of the $M_\bullet - \sigma$ relation

- To unbind the bulge in one crossing time ($\frac{R_{Bulge}}{\sigma}$) by a black hole radiating at Eddington limit the condition is :

$$L_E \times t_{cross} \approx L_E \times \frac{R_{Bulge}}{\sigma} \approx \frac{GM^2_{Bulge}}{R_{Bulge}}$$

- Eddington Luminosity :

$$L_E = \frac{4\pi G M_\bullet m_p c}{\sigma_e}$$

- From virial theorem, $GM_{Bulge} \approx \sigma^2 R_{Bulge}$.
- Therefore,

$$M_\bullet \approx \frac{\sigma_e \sigma^5}{4\pi G^2 m_p c} \approx 3 \times 10^5 \left(\frac{\sigma}{200 kms^{-1}}\right)^5 M_\odot.$$

Significance of the $M_\bullet - \sigma$ relation

- Momentum driven flow : The energy released by the SBH is lost to radiation and few percent of it affects the bulge gas mechanically.
- If the optical depth is of the order of unity the momentum of the outflow is comparable to the photon momentum :

$$\dot{M}v \approx \frac{L_E}{c}$$

- For a shell of gas of radius $R(t)$ and mass $f_g M(R)$ ($M(R)$ is the total mass including the star and the gas within radius R, f_g is the gas fraction)which has been swept up by the flow, the equation of motion is : (King., 2003)

$$\frac{d}{dt}\left[f_g M(R)\dot{R}\right] + \frac{G f_g M(R)[M_\bullet + M(R)]}{R^2} = \frac{L_E}{c}.$$

Significance of the $M_\bullet - \sigma$ relation

- For isothermal sphere consideration, this reduces to,

$$\frac{d}{dt}(R\dot{R}) + \frac{GM_\bullet}{R} = -2\sigma^2\left(1 - \frac{M_\bullet}{M_\sigma}\right)$$

- Critical mass :

$$M_\sigma \equiv \frac{f_g \sigma_e}{\pi G^2 m_p}\sigma^4 \approx 2 \times 10^8 \left(\frac{f_g}{0.1}\right)\left(\frac{\sigma}{200 kms^{-1}}\right)^4 M_\odot$$

- For $M_\bullet < M_\sigma$, RHS of the equation becomes negative.
- For large r, the third term in the LHS can be neglected. Therefore we finally have, $\frac{d}{dt}(R\dot{R}) = -ve$, which in turn implies that force on the shell is unable to lift it beyond a certain radius.
- Therefore this equation does not have any solution under these conditions.

Significance of the $M_\bullet - \sigma$ relation

- If $M_\bullet > M_\sigma$, RHS becomes positive implying that $\dot{R}^2 + R\ddot{R} = \sigma^2 \times constant$.
- When the gas stops accelerating $\dot{R}$ becomes constant making the second term to be zero and $\dot{R}^2 \rightarrow \sigma^2$.
- The shell can be expelled completely.
- Upper limit to $M_\bullet \Rightarrow$ For active galaxies $M_\bullet < M_\sigma$.
- the critical mass is larger by a factor of $\sim \frac{c}{\sigma}$.
- In the ”momentum driven flow” there is sufficient cooling process which causes a large percentage of that energy to be lost in radiation.

Significance of the $M_\bullet - \sigma$ relation

- Consumption of stars : The SBHs can also grow by consumption of stars. This consumption can be in two ways.
- The stars those passes within the event horizon can be directly captured.
- The indirect capture occurs when consumption is done by accreting the gas from tidally disrupted stars.
- For a singular isothermal sphere $\rho = \frac{\sigma^2}{2\pi G R^2}$ and $M(r) = \frac{2\sigma^2 r}{G}$.
- The rate at which stars carry mass past a sphere of radius r while moving along their orbits can be written as :

$$\sim 4\pi r^2 \sigma \rho \approx 4\pi r^2 \frac{\sigma^2}{2\pi G R^2} \sigma \approx \frac{2\sigma^3}{G}.$$

Significance of the $M_\bullet - \sigma$ relation

- The fraction $\frac{r_{lc}}{r}$ of stars moving in the orbits will go within the distance r_{lc} of the SBH.
- Putting $r = r_h$ (radius of influence) and r_{lc} to be a multiple of gravitational radius of SBH ($r_g = \frac{GM_\bullet}{c^2}$) (This is because for capture by massive black holes $r_g \leq r_{lc} \leq 10 r_g$), the accretion rate can be written as :

$$\dot{M} = \frac{2\sigma^3}{G}\frac{r_{lc}}{r_h} \approx 10\frac{\sigma^5}{Gc^2}.$$

- Therefore, after 10 Gyr, the total mass that will be accumulated is:

$$M_\bullet = 1 \times 10^8 \left(\frac{\sigma}{200 kms^{-1}}\right)^5 M_\odot.$$

- This is also in agreement with the observed relation of $M_\bullet$ - σ.

Significance of the $M_\bullet - \sigma$ relation

- The fraction of stars in isothermal distribution captured by a Schwarzchild black hole is

$$f(r) \simeq (J_{cap}/2\sigma r)^2,$$

- where, $J_{cap} = \frac{4Gm}{c}$ is the maximum angular momentum for capture (Zhao, Haenelt & Rees 2002).
- This translates into an energy flux $\propto \rho(r_h) r_h^2 \sigma f(r_h)$ which also results in $p = 5$.

Plan of talk

- Active vs quiescent nuclei
- Stellar dynamics
- Gas dynamics
- Accretion dynamics and light curve profile
- Detections and event rate predictions
- Summary and conclusions
- Future projects

Active Vs quiescent galaxies

Active

Some galaxies exhibit evidence of extremely violent processes taking place within them. Active Galaxies are galaxies characterized by certain properties:

- High luminosity $\sim 10^{45}$ erg $\sec^{-1}$
- Accretion disk leading to thermal and non thermal emission
- Strong emission lines in the spectra
- Rapid variability
- Jets

Quiescent

Most of the galaxies are quiescent indicating that any central massive black holes present is starve of fuel and will be detectable only through its gravitational influence on the stars in host galaxy.

- Tidal disruption of stars due to tidal gravity by black hole.
- Gravitational waves due to star orbiting around black holes (EMRI).

  Frequency: $10^{-4} - 10^{-1}$ Hz.

  Detectable missions: eLISA

Stellar Dynamics around black holes

Topics

- Physical radii
- Loss cone dynamics
- Fokker-Planck equation
- Theoretical capture rate

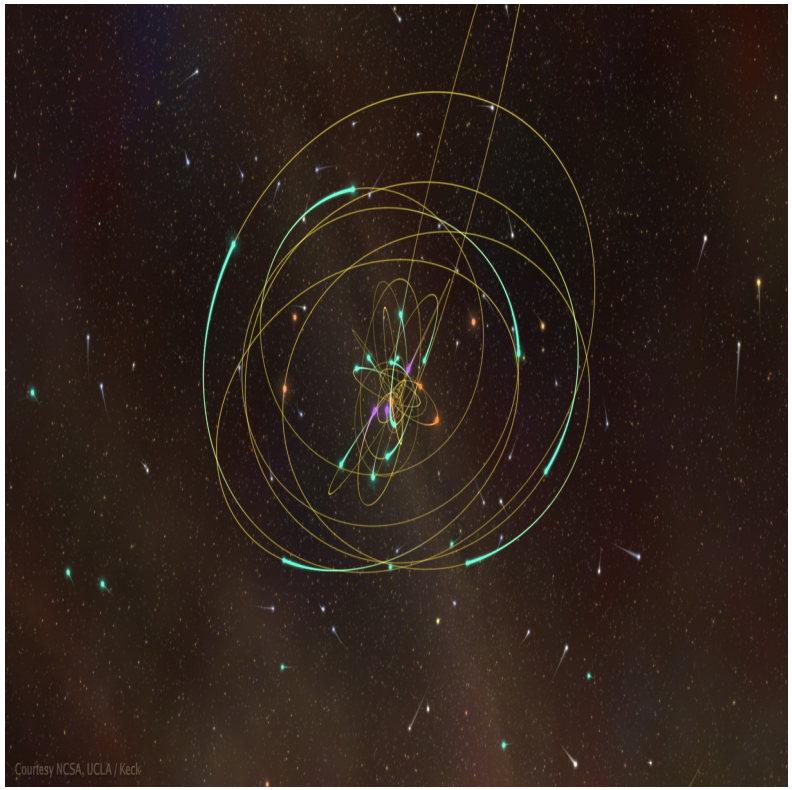

Relevant radii

- Schwarzschild radius:

$$R_s = 3 \times 10^5 \left(\frac{M_\bullet}{M_\odot}\right) \mathrm{cm}$$

- Radius of influence, r_h:

$$r_h = \frac{GM_\bullet}{v_c^2}$$

- Tidal radius:

$$r_t \simeq 1.4 \times 10^{11} \left(\frac{M_\bullet}{M_\odot}\right)^{1/3} \mathrm{cm}$$

- Critical mass is implied and is given by $r_t = R_s$. For solar type stars

$$M_c \simeq 3 \times 10^8 M_\odot \frac{R_\star}{R_\odot} \frac{M_\star}{M_\odot}$$

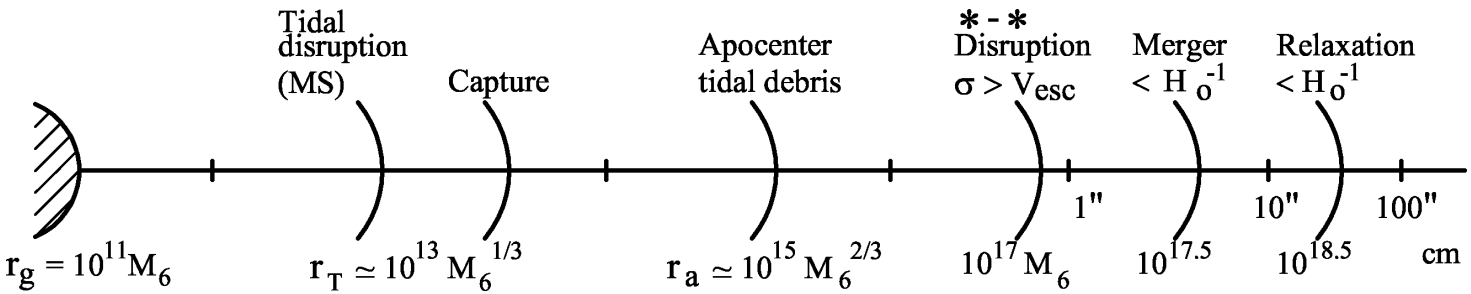

Figure: Radii of physical importance.

Stellar Dynamics

For a isotropic galaxy with dominated black hole potential, the distribution function $f(E) \propto E^p \Rightarrow$ number density $n(r) \propto r^{-p-\frac{3}{2}}$ where $E = \psi(r) - 0.5v^2$.

Peebles 1972: Number flux remains constant

$$\frac{n(r)r^3}{t_R(r)} = \text{const}; \quad n(r) \propto r^{-9/4}; \quad p = \frac{3}{4}$$

Bahcall & Wolf 1976: Gravitational scattering in calculation and energy flux constant

$$\frac{n(r)r^3}{t_R(r)}v^2 = \text{const}; \quad n(r) \propto r^{-7/4} = const; \quad p = \frac{1}{4}$$

leads to $n(r) \propto r^{-7/4}$. This is called as "**Bahcall-Wolf Cusp**'

Loss Cone dynamics

A loss cone is a theoretical cone or a set of velocity vectors, at some distance r from the SMBH such that a star whose orbit passes through the cone is captured by the black hole.

Angular momentum of the orbit

$$J^2 \leq J_{lc}^2 = 2r_{lc}^2(\Psi(r_{lc}) - E)$$

where $r_{lc} = r_t$ is the loss cone radius and J_{lc} is the loss cone angular momentum.

For highly eccentric orbit, loss cone angle is given by [Frank & Rees 1976]

$$\theta_{lc} \approx \begin{cases} (2r_{lc}/3r)^{1/2} & r \leq r_h \\ (2r_{lc}r_h)^{1/2}/r & r \geq r_h \end{cases}$$

The capture rate can be given by

$$\dot{N} \approx \frac{N_{lc}}{t_{dyn}} \approx \frac{n(r)r^3}{t_R}$$

where t_R is the relaxation time of the galaxy.

Loss cone dynamics

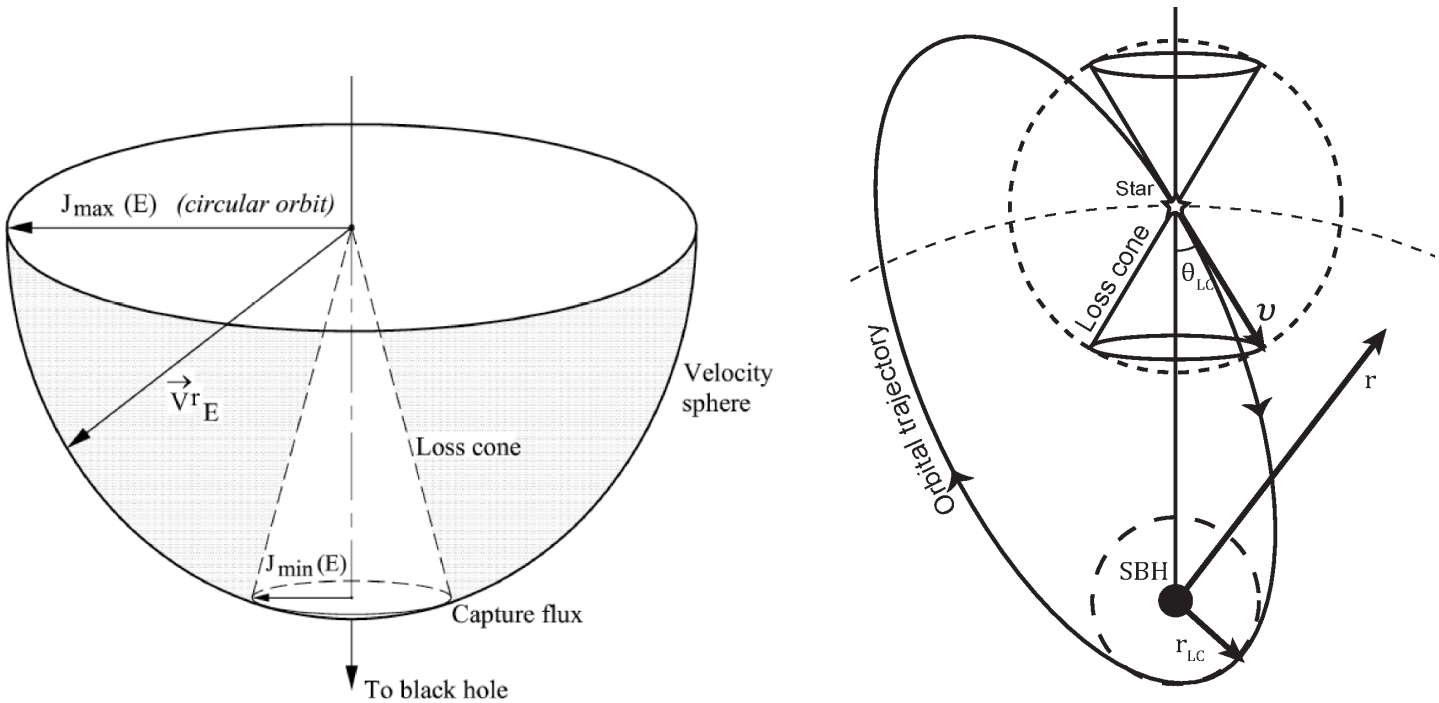

Figure: Loss cone orbits in (Left) Velocity space (Right) Real space.

Source: (a) Lightman & Shapiro 1977 (b) Merritt 2013 (Review article: Loss cone dynamics).

Fokker-Planck in phase space

Orbit of stars can be diffused into the loss cone either by change in the energy of star or by change in angular momentum of the orbit or by both [Rosenbluth 1957; Lightman & Shapiro 1977].

$$\frac{\partial}{\partial t}(g\, f(x^\alpha, v^\alpha, t)) = -\frac{\partial}{\partial v^\alpha}(< \Delta v^\alpha > g\, f) + \frac{1}{2}\frac{\partial^2}{\partial v^\alpha \partial v^\beta}(< \Delta v^\alpha \Delta v^\beta > g\, f)$$

where $f(x^\alpha, v^\alpha, t)$ is the distribution function, v^α are the velocity space coordinates, density of state $g = |g_{ab}|$ where g_{ab} is the metric tensor in velocity space.

Diffusion coefficients in terms of Rosenbluth potentials [Rosenbluth et al. 1957].

$$h(v) = \int \frac{f(v_f)}{|v - v_f|}\, d^3 v_f \qquad < \Delta v_i >= 4\pi G^2 \ln\Lambda M_f (M + M_f)\frac{\partial}{\partial v_i} h(v)$$

$$g(v) = \int f(v_f)|v - v_f|\, d^3 v_f \qquad < \Delta v_i \Delta v_j >= 4\pi G^2 \ln\Lambda\, M_f^2 \frac{\partial}{\partial v_i \partial v_j} g(v)$$

where M_f, M, $f(v_f)$ are mass of field stars, mass of stars and field stars distribution.

Flow chart

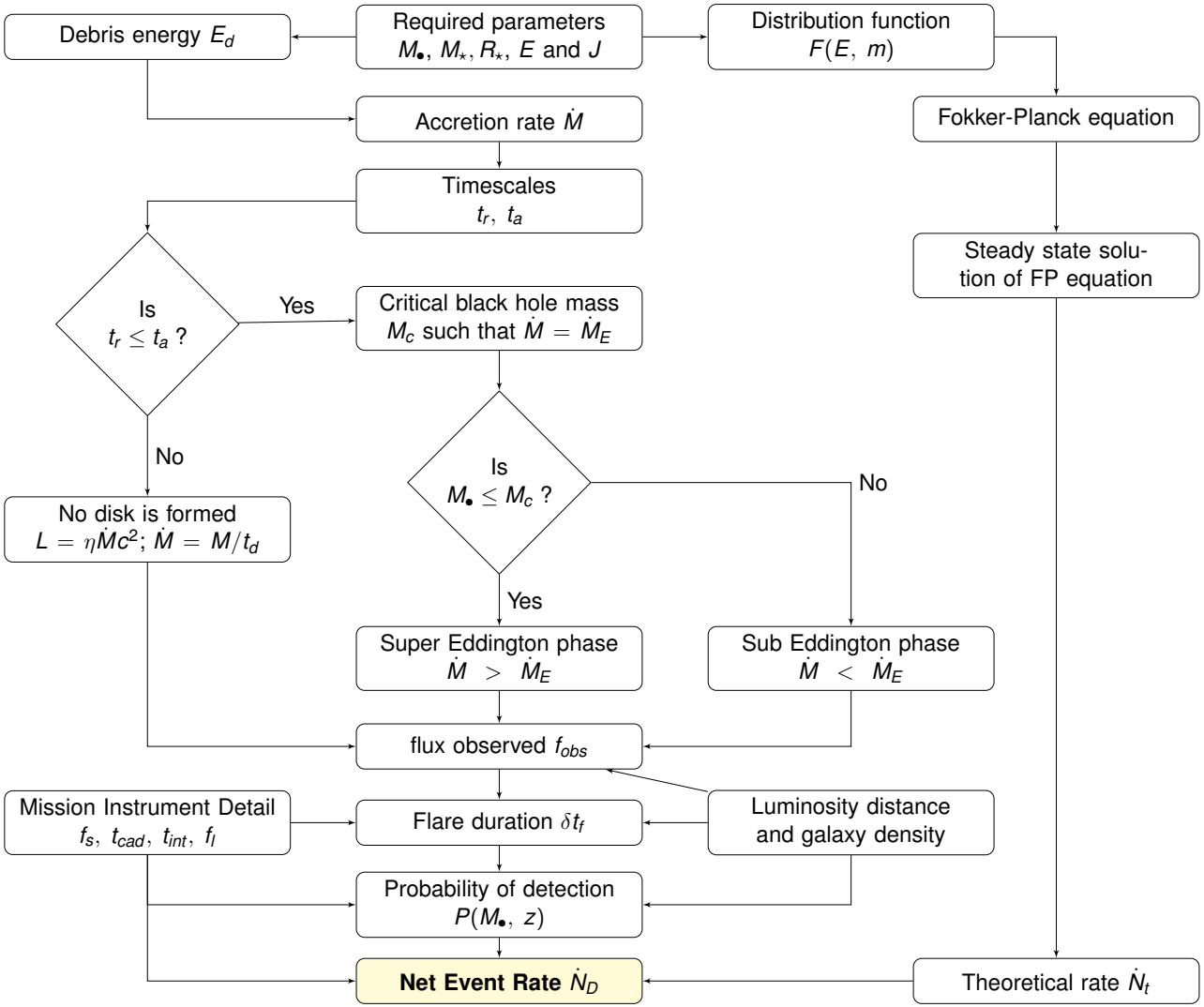

Figure: The flow chart of the procedure we have adopted in the calculation of event rates is shown. The stellar dynamics and gas dynamics are connected by the parameters of specific energy E and specific angular momentum J of the star's initial orbit.

Distribution function (DF) and mass function

We consider the distribution function

$$F(E,\ m) = f(E)\xi(m) \tag{2}$$

where $m = M_\star/M_\odot$ and ξ is the mass function (MF) of star's cluster. The mass function is given by (Kroupa et al. 2001)

$$\xi(m) \approx \begin{cases} Am^{-1.3} & 0.08 < m < 0.5 \\ Bm^{-2.3} & 0.5 < m < 150 \end{cases}$$

where

$$A = 2B \quad \& \quad B = \frac{1}{7.91 - 0.77 m_m^{-1.3}}$$

where m_m is the maximum mass of star in the cluster taken to be 150.

Stellar structure and mass limit

Life time of main sequence (MS) star

$$t_{MS} \approx t_{\odot} \left(\frac{M_{\star}}{M_{\odot}} \right)^{-2.5}$$

where $t_{\odot} \sim 10^{10}$ Yr.

The dynamical time of the star to fall into the black hole

$$t_d = \sqrt{\frac{a^3}{GM_{\bullet}}}$$

For star to be captured as a main sequence,

$$t_d < t_{MS} \quad \Rightarrow \quad \frac{M_{\star}}{M_{\odot}} < m_l = \left(t_{\odot} \sqrt{\frac{GM_{\bullet}}{a^3}} \right)^{0.4}$$

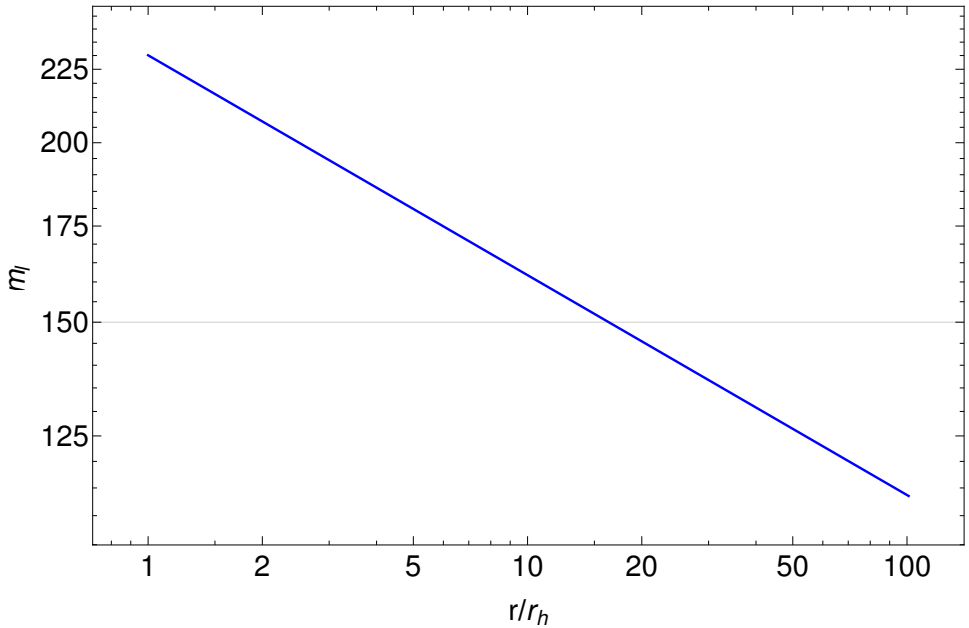

Distribution function: $f(E)$

Density: $\rho(r) \propto r^{-\gamma}$

Stellar potential

$$\Phi_\star(r) = \frac{2}{2-\gamma}\sigma^2\left[1-\left(\frac{r}{r_h}\right)^{2-\gamma}\right]$$

Total potential

$$\Phi(r) = \frac{GM_\bullet}{r} + \Phi_\star(r)$$

Eddington formula

$$f(E) = \frac{1}{\sqrt{8}\pi^2\langle M_\star\rangle}\frac{\mathrm{d}}{\mathrm{d}E}\int_{E_{min}}^{E}\frac{\mathrm{d}\rho}{\mathrm{d}\Phi}\frac{1}{\sqrt{E-\Phi}}\,\mathrm{d}\Phi,$$

where $\langle M_\star\rangle = \int_{0.08}^{150} M_\star\ \xi(m)\,\mathrm{d}m$

Thus, distribution function is

$$\boxed{f(\mathcal{E}) = \frac{M_\bullet}{\langle M_\star\rangle}\frac{1}{r_h^3\sigma^3}g(\mathcal{E})}; \quad \mathcal{E} = \frac{E}{\sigma^2}$$

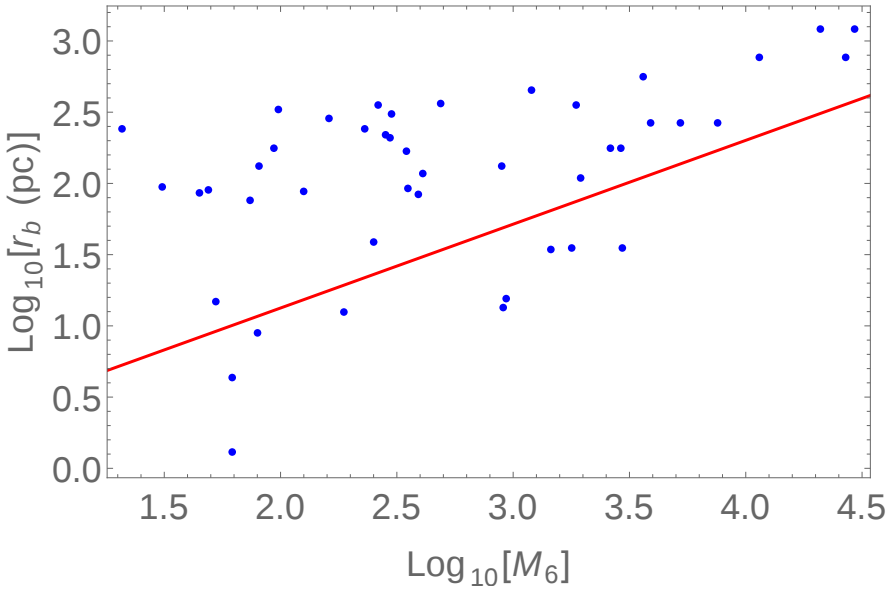

Blue points are break radius for Nuker profile (Wang & Merritt 2004) and red line is radius of influence r_h. $M_\bullet$–σ relation is given by

$$M_\bullet = 1.66\times10^8 M_\odot\left(\frac{\sigma}{200\ \mathrm{Km\ sec^{-1}}}\right)^{4.86}$$

Distribution function: $f(E)$

$$g(\mathcal{E}) = \frac{\gamma(3-\gamma)}{2\sqrt{8}\pi^3}\frac{\mathrm{d}}{\mathrm{d}\mathcal{E}}\int_{x_1}^{x_2}\frac{x^{\gamma-1}}{\sqrt{\mathcal{E}-x-\frac{2}{2-\gamma}(1-x^{\gamma-2})}}\,\mathrm{d}x$$

where $x = \frac{r_h}{r}$ and

$$x_1 + \frac{2}{2-\gamma}(1-x_1^{\gamma-2}) = \mathcal{E}_{min}$$

$$x_2 + \frac{2}{2-\gamma}(1-x_2^{\gamma-2}) = \mathcal{E}$$

The distribution function

$$\boxed{F(E,\ m) = f(E)\xi(m)}$$

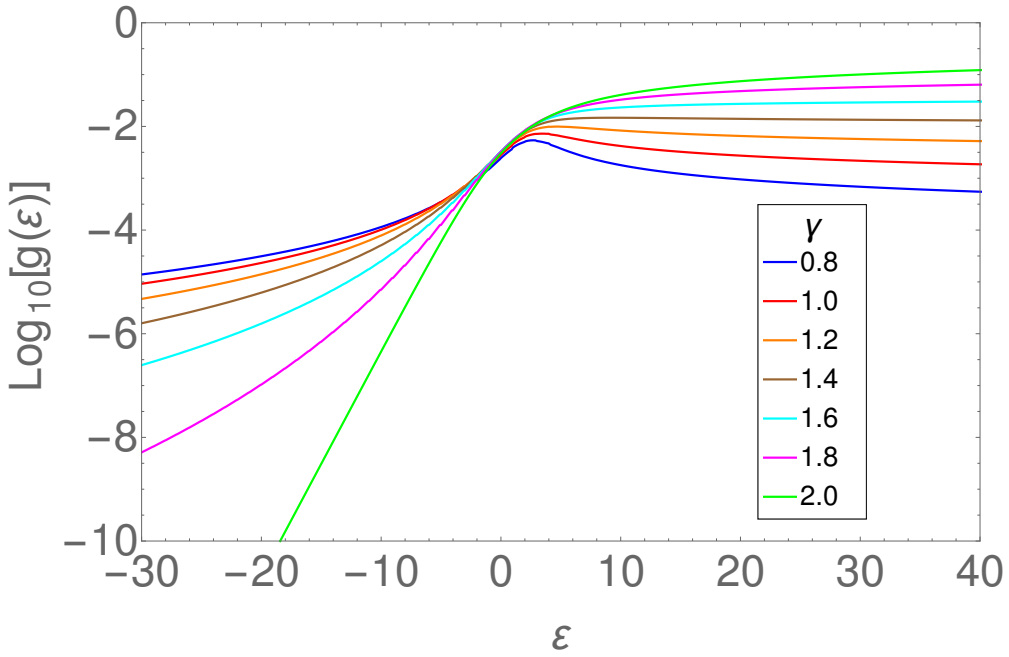

Fokker- Planck equation

In $\mathcal{E}$ and $j = J^2/J_c^2$ space where J_c is circular angular momentum, the Fokker- Planck equation in limit $j \to 0$ reduces to

$$\frac{\mathrm{d}\mathcal{F}(\chi,\ y)}{\mathrm{d}\chi} = \frac{\mathrm{d}}{\mathrm{d}y}\left(y\frac{\mathrm{d}\mathcal{F}(\chi,\ y)}{\mathrm{d}y}\right)$$

with the boundary condition

$$\begin{aligned} \mathcal{F}(0,\ y) &= 0 \qquad\qquad \forall\ \ y < y_{lc} \\ \mathcal{F}(0,\ y) &= \mathcal{F}(1,\ y) \quad \forall\ \ y \geq y_{lc} \end{aligned}$$

where

$$\chi = \frac{1}{\langle D(\mathcal{E})\rangle}\int_{r_p}^{r}\lim_{j\to 0}\frac{\left\langle(\Delta j)^2\right\rangle}{2j}\frac{\mathrm{d}r}{v_r} \quad , \quad y = \frac{j}{\langle D(\mathcal{E})\rangle}$$

and $\langle D(\mathcal{E})\rangle$ is the orbit averaged diffusion coefficient given by (Binney & Tremaine 2008)

$$\langle D(\mathcal{E})\rangle = \frac{32\sqrt{2}}{3}\frac{\pi^2 G^2\left\langle M_f^2\right\rangle \log\Lambda}{J_c^2(\mathcal{E})}\frac{M_\bullet}{\langle M_\star\rangle}\frac{1}{\sigma^2}(2h_1(\mathcal{E}) + 3h_2(\mathcal{E}) - h_3(\mathcal{E})) \qquad (5)$$

where M_f is the mass of field star, $\Lambda \approx M_\bullet/M_\star$.

Diffusion coefficients

$$\left\langle M_f^2 \right\rangle = M_\odot^2 \int_{0.08}^{150} m_f^2 \xi(m_f)\, \mathrm{d}m_f$$

$$h_1(\mathcal{E}) = \int_0^{s(\mathcal{E})} \mathrm{d}s' \frac{s'^2}{\sqrt{\Psi(s') - \mathcal{E}}} \int_{-\infty}^{\mathcal{E}} \mathrm{d}\mathcal{E}'\ g(\mathcal{E}')$$

$$h_2(\mathcal{E}) = \int_0^{s(\mathcal{E})} \mathrm{d}s' \frac{s'^2}{\Psi(s') - \mathcal{E}} \int_{\mathcal{E}}^{\Psi(s's)} \mathrm{d}\mathcal{E}' \sqrt{\Psi(s') - \mathcal{E}'}\ g(\mathcal{E}')$$

$$h_3(\mathcal{E}) = \int_0^{s(\mathcal{E})} \mathrm{d}s' \frac{s'^2}{(\Psi(s') - \mathcal{E})^2} \int_{\mathcal{E}}^{\Psi(s')} \mathrm{d}\mathcal{E}' (\Psi(s') - \mathcal{E}')^{\frac{3}{2}}\ g(\mathcal{E}')$$

where $s(\mathcal{E})$ is obtained by solving $\Psi(s) = \mathcal{E}$, $s = r/r_h$ and

$$\Psi(s) = \frac{\Phi}{\sigma^2} = \frac{1}{s} + \frac{2}{2-\gamma}(1 - s^{2-\gamma}). \tag{7}$$

Now $J_c^2(\mathcal{E})$ is given by

$$J_c^2(\mathcal{E}) = \sigma^2 r_h^2\ [s_c(\mathcal{E}) + 2s_c^{4-\gamma}(\mathcal{E})] \qquad \text{where} \qquad \frac{1}{2s_c} + \frac{2}{2-\gamma}(1 - s_c^{2-\gamma}) - s_c^{2-\gamma} = \mathcal{E}. \tag{8}$$

Theoretical capture rate

Solution of Fokker- Planck equation is

$$\mathcal{F}(\chi,\ y) = X(j_{lc}) \left(1 - 2 \sum_{n=1}^{\infty} \frac{e^{\frac{-\alpha_n^2 q}{4}\chi}}{\alpha_n} \frac{J_0\left(\alpha_n \sqrt{y/y_{lc}}\right)}{J_1(\alpha_n)} \right) \tag{9}$$

where α_n are the consecutive zeros of the Bessel function $J_0(\alpha)$, $q = 1/y_{lc}$ and $X(j_{lc})$ is given by

$$X(j_{lc}) = \frac{f(\mathcal{E})}{1 + q^{-1}\zeta(q) \log\left(\frac{1}{j_{lc}}\right)};\ \zeta(q) = 1 - 4 \sum_{n=1}^{\infty} \frac{e^{\frac{-\alpha_n^2 q}{4}}}{\alpha_n^2}$$

The $\zeta(q)$ is approximated by

$$\zeta(q) \approx \begin{cases} 1 & q \geq 4 \\ \dfrac{q}{0.86q^{0.5} + 0.384q - 0.379q^{1.5} + 0.427q^2 - 0.095q^{2.5}} & q < 4 \end{cases}$$

Theoretical capture rate

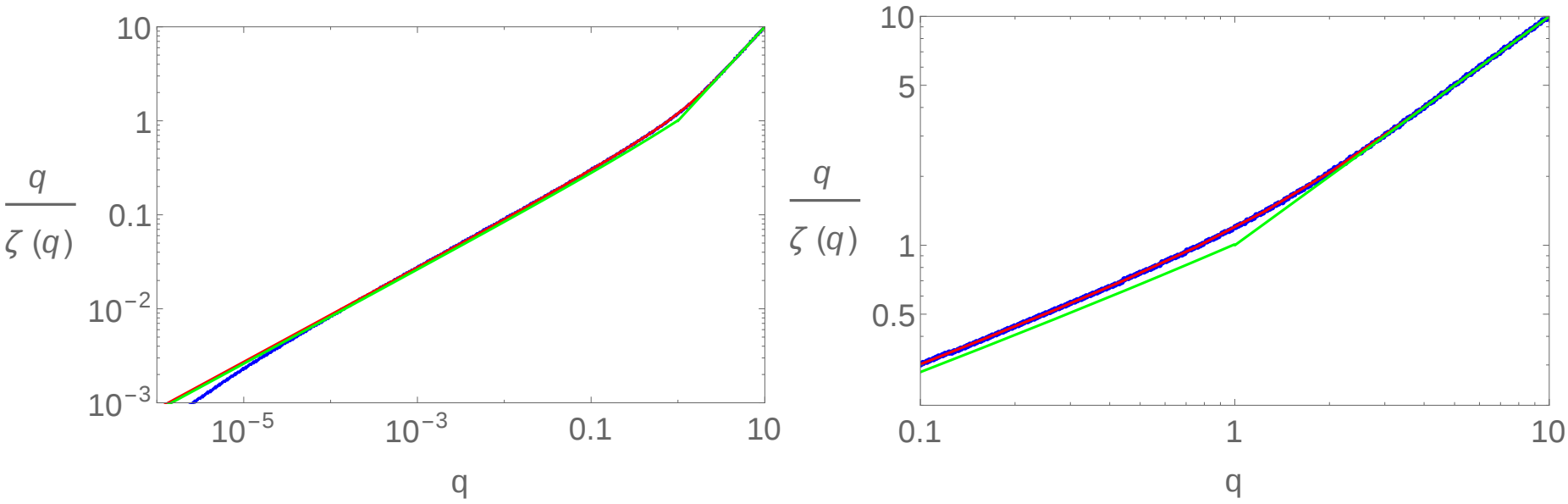

Figure: Shows $q/\zeta(q)$ as a function of q over all ranges under various approximations. The blue line corresponds to $\zeta(q)$ summed upto 10000 terms. The red thin line corresponds to our approximation of $\zeta(q)$. The green line shows the results obtained by Cohn & Kulsrud (1978). Asymptotically terms in $\zeta(q)$, the blue line follows the red thin line. The figure (b) shows $q/\zeta(q)$ that for q close to unity, our approximated formula gives good fit to $\zeta(q)$.

Theoretical capture rate

The loss cone feeding rate is given by Merritt (2013)

$$\frac{\mathrm{d}^2\dot{N}_t}{\mathrm{d}\mathcal{E}\ \mathrm{d}y} = 4\pi^2\sigma^2 \int \mathrm{d}m\, \xi(m) J_c^2(E) \langle D(E)\rangle \mathcal{F}(\chi = 1,\ y) \tag{10}$$

The Jacobian of the transformation from $\{\mathcal{E},\ y\}$ space to dimensionless variables $\{\mathcal{E},\ \ell^2 = (J/J_{lc}(\mathcal{E}, r_t))^2 = j(J_c(\mathcal{E})/J_{lc}(\mathcal{E}, r_t))^2\}$ is given by

$$\mathrm{d}\mathcal{E}\ \mathrm{d}y = \frac{J_{lc}^2(\mathcal{E}, r_t)}{\langle D(\mathcal{E})\rangle\, J_c^2(\mathcal{E})} \mathrm{d}\mathcal{E}\ \mathrm{d}\ell^2 \tag{11}$$

Then, the feeding rate is given by

$$\frac{\mathrm{d}^2\dot{N}_t}{\mathrm{d}\mathcal{E}\ \mathrm{d}\ell^2} = 4\pi^2\ \ \sigma^2 \int \mathrm{d}m\, \xi(m)\ J_{lc}^2(\mathcal{E})\ \ \mathcal{F}(\chi = 1,\ \ell) \tag{12}$$

Capture constraints on phase space

The orbital motion of a star at the turning points of the orbit r_x, is given by

$$E = \Phi(r_x) - \frac{J^2}{2r_x^2}$$

In terms of dimensionless variables $\ell = J/J_{lc}$ and $\bar{e} = E/E_m$ where $E_m = GM_\bullet/r_t$

$$\frac{\bar{e}}{s_t} = \frac{s_x - \ell^2 s_t + \frac{2}{2-\gamma}\left[s_x^2(1 - s_x^{2-\gamma}) - \ell^2 s_t^2(1 - s_t^{2-\gamma})\right]}{s_x^2 - \ell^2 s_t^2} \tag{13}$$

where $s_x = r_x/r_h$, $s_t = r_t/r_h$. Since $\bar{e}$ is a monotonically decreasing function of s_x and both the pericenter and apocenter of the orbit should lie below r_h, the minimum value of $\bar{e}$ is at $s_x = 1$ for $r_x = r_h$; taking $\bar{e}(s_x = 1) = \bar{e}_h$, the eqn (13) reduces to

$$\frac{\bar{e}_h}{s_t} = \frac{1 - \ell^2 s_t - \frac{2}{2-\gamma}\ell^2 s_t^2(1 - s_t^{2-\gamma})}{1 - \ell^2 s_t^2}.$$

Since,

$$s_t = r_t/r_h \sim 10^{-5} - 10^{-6} \quad \Rightarrow \quad \boxed{\bar{e}_h \simeq r_t/r_h} \tag{14}$$

Capture constraints on phase space

As $s_t = r_t/r_h \sim 10^{-5} - 10^{-6}$, total potential is dominated by the black hole. Ignoring second term in eqn (13)

$$\bar{e} = \frac{x_x - \ell^2}{x_x^2 - \ell^2}; \qquad x_x = \frac{s_x}{s_t}$$

The roots are given by

$$x_x = \frac{1}{2\bar{e}}\left(1 \pm \sqrt{1 - 4\bar{e}(1-\bar{e})\ell^2}\right)$$

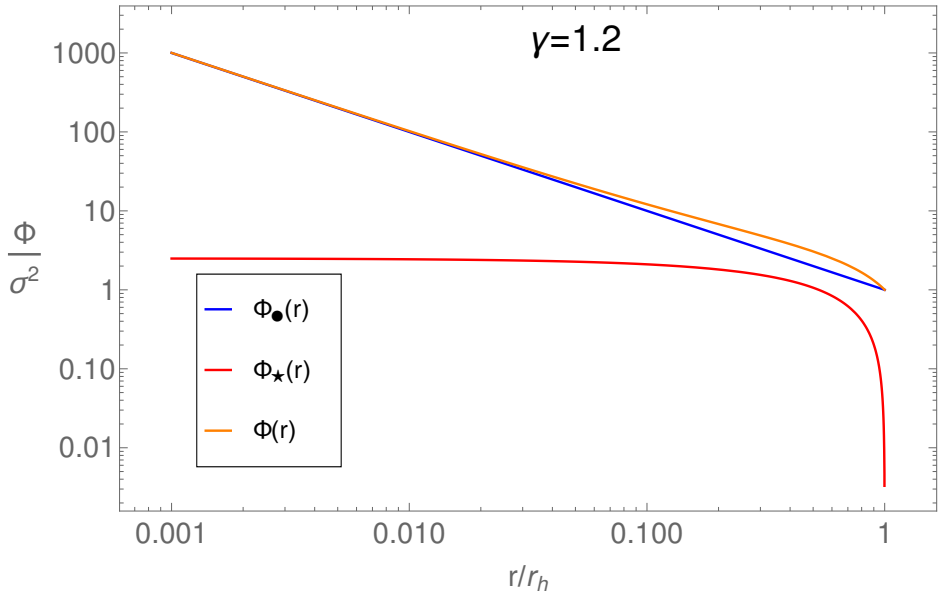

Pericenter of the orbit is

$$x_p = \frac{1}{2\bar{e}}\left(1 - \sqrt{1 - 4\bar{e}(1-\bar{e})\ell^2}\right); \qquad x_p = \frac{r_p}{r_t} \tag{15}$$

$$x_p < 1 \quad \Rightarrow \quad (1-\bar{e})(1-\ell^2) > 0; \quad x_p > 0 \quad \Rightarrow \quad \ell^2\bar{e}(1-\bar{e}) > 0$$

Thus, the applicable ranges are

$$\boxed{\bar{e}_h < \bar{e} < 1, \quad 0 < \ell < 1}$$

Probability of main sequence star capture

The radial period of an orbit is given by

$$T_r = \int_{r_p}^{r_a} \frac{1}{v_r} \mathrm{d}r.$$

which in terms of $s = r/r_h$ is given by

$$T_r = \frac{r_h}{\sqrt{2}\sigma} \int_{s_p}^{s_a} \frac{s\sqrt{s_t}}{\sqrt{s_t\left(s - \ell^2 s_t + \frac{2}{2-\gamma}\left[s^2(1-s^{2-\gamma}) - \ell^2 s_t^2(1-s_t^{2-\gamma})\right]\right) - \bar{e}(s^2 - \ell^2 s_t^2)}} \mathrm{d}s,$$

where s_a and s_p are the dimensionless apocenter and pericenter. We find numerically that the radial period T_r is approximated by

$$T_r(\bar{e},\ M_\bullet,\ m) \simeq \frac{\pi}{2\sqrt{2}} \frac{r_h}{\sigma} \begin{cases} 0.57 e^{[0.27(1.47 - \frac{\bar{e}}{s_t})]} & \bar{e} < 1.47 s_t \\ \left(\frac{\bar{e}}{s_t}\right)^{-\frac{3}{2}} & \bar{e} \geq 1.47 s_t \end{cases}$$

A tidally captured star is on main sequence if its main sequence lifetime $t_{MS} > T_r$ where T_r is the radial period of the orbit. Considering all possible radial phases of the star in an orbit, the probability that a star of mass m is tidally captured as a main sequence is given by

$$f_\star(\bar{e},\ M_\bullet,\ m) = \mathrm{Min}\left[1,\ \frac{t_{MS}(m)}{T_r(\bar{e},\ M_\bullet,\ m)}\right].$$

Theoretical capture rate

In the black hole mass range $M_6 = 1 - 100$,

- $m < 0.8$: a substantial fraction of stars are tidally captured without disruption.
- $m > 0.8$: all stars are tidally disrupted.

Thus, the star mass range is taken to be

$m = 0.8 - 150$.

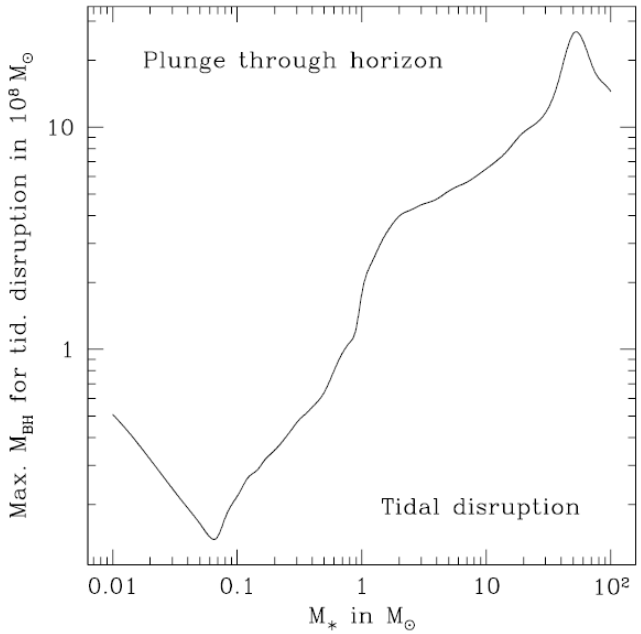

Frietag & Benz (2002)

In terms of $\bar{e} = s_t \mathcal{E}$ and ℓ, the capture rate is given by

$$\frac{\mathrm{d}^2 \dot{N}_t}{\mathrm{d}\bar{e}\ \mathrm{d}\ell^2\ \mathrm{d}m} = 4\pi^2\ \ s_t^{-1}\sigma^2\ \ \xi(m) f_\star(\bar{e},\ M_\bullet,\ m)\ J_{lc}^2(\bar{e})\ \ \mathcal{F}(\chi = 1,\ \ell).$$

The net capture rate integrated over $\bar{e}$, ℓ and m is given by

$$\dot{N}_t(\gamma,\ M_\bullet) = 4\pi^2 \int_{0.8}^{150} \mathrm{d}m \int_{\bar{e}_h}^{1} \mathrm{d}\bar{e} \int_0^1 \mathrm{d}\ell^2\ \ \sigma^2 s_t^{-1}(M_\bullet,\ m)\xi(m) f_\star(\bar{e},\ M_\bullet,\ m)\ J_{lc}^2(\bar{e})\ \ \mathcal{F}(\chi = 1,\ \ell).$$

Theoretical capture rate

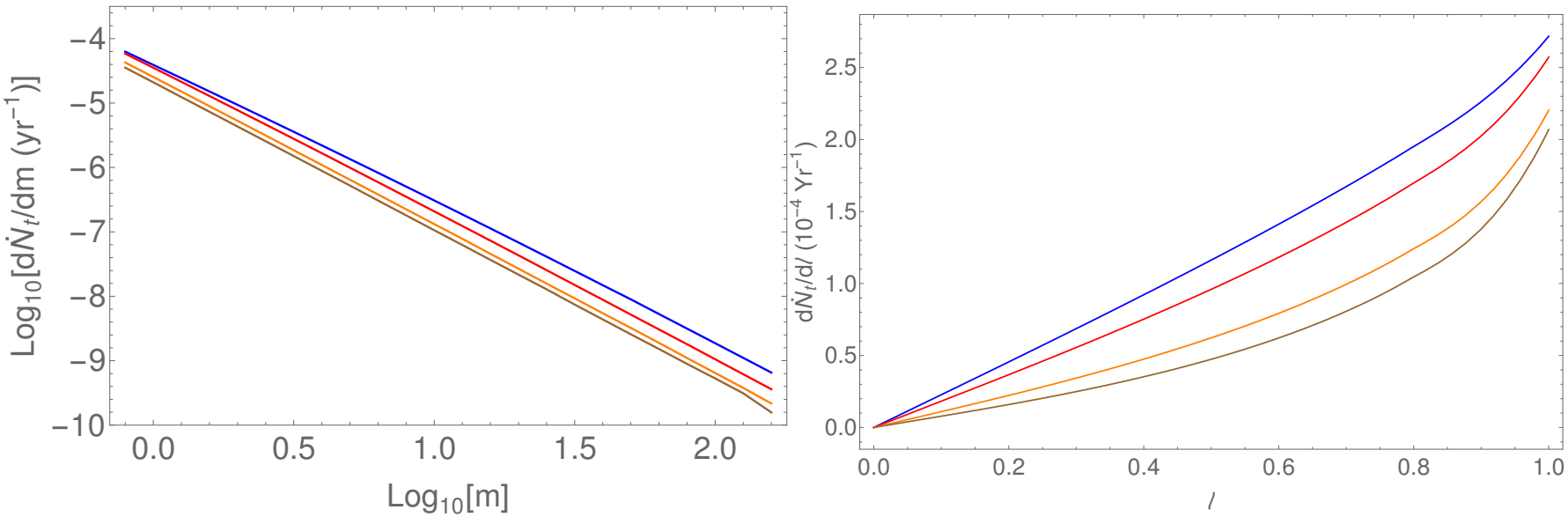

Figure: (Left) shows $\dot{N}_t$ per m integrated over $\bar{e}$ and ℓ. The $\xi(m)$ decreases with m and thus $\dot{N}_t$ decreases with m. (Right) shows the $\dot{N}_t$ per ℓ integrated over $\bar{e}$ and m.

Theoretical capture rate

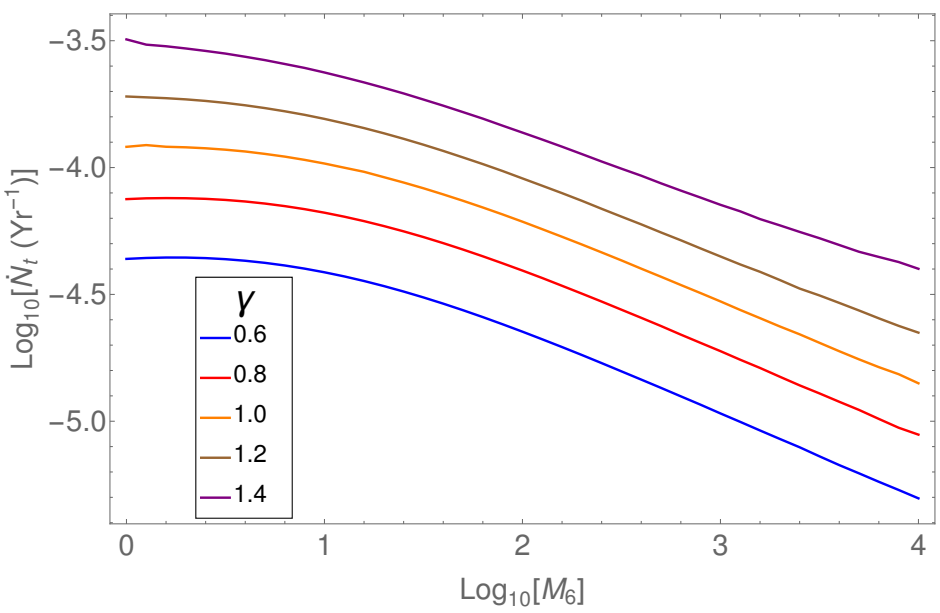

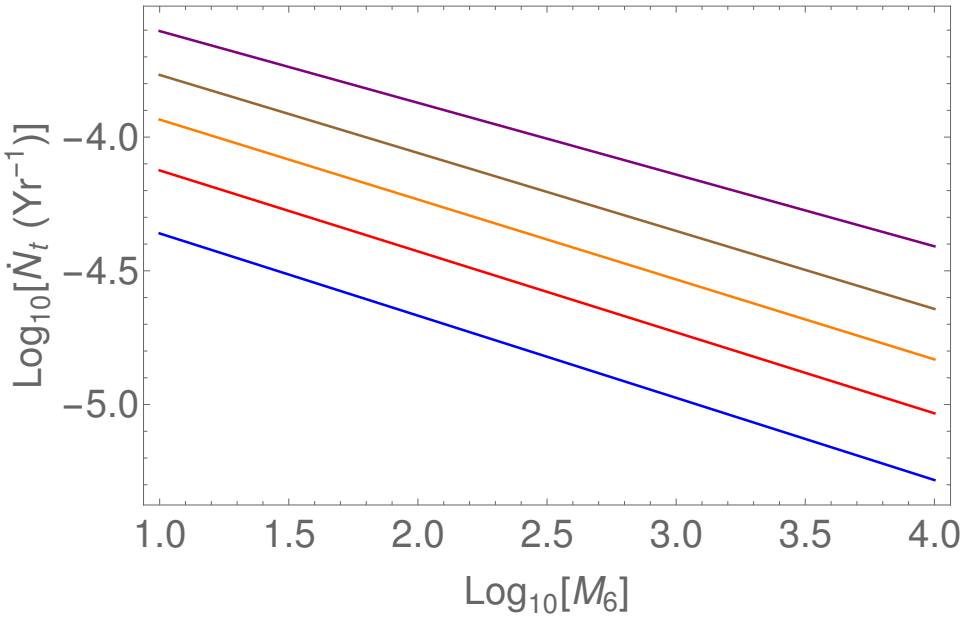

Figure: (Left) shows the net $\dot{N}_t$ integrated over $\bar{e}$, ℓ and m as a function of M_6 for various γ and does not show a power law relation for $M_6 < 10$. (Right) shows $\dot{N}_t$ as a function of M_6 for $M_6 > 10$ and it follows that $\dot{N}_t \propto M_6^{\beta}$ where $\beta = 0.3 \pm 0.01$.

Theoretical capture rate

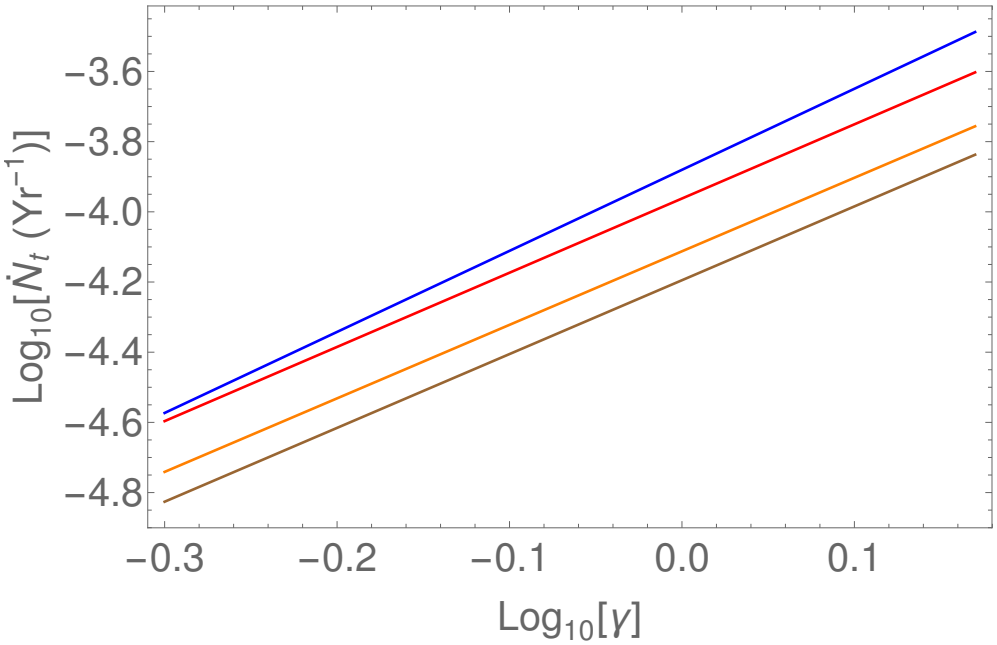

Figure: The figure shows the $\dot{N}_t$ as a function of γ for various M_6=1 (blue), 10 (red), 50 (orange) and 100 (brown) and it follows $\dot{N}_t \propto \gamma^p$ with the best fit value of $p \sim 2.1$. The $\dot{N}_t$ increases with γ due to increase in the density of central stellar population.

Physics of Tidal Disruption

Topics

- Stellar disruption
- Accretion rate
- Formation of disk
- Eddington rate

Accretion rate

The stars on the loss cone orbits are captured within the dynamical time $t_d = (r_p^3/GM_\bullet)^{0.5}$ with tidal acceleration $a_t = GM_\bullet \Delta R/r_p^3$ where ΔR is the debris distance from the star center at the moment of breakup. Then, the energy of the disrupted debris is given by

$$E_d(\bar{e},\ \ell,\ M_\bullet,\ m,\ \Delta R) \approx \bar{e}E_m - \frac{2kGM_\bullet \Delta R}{r_p^2} \tag{16}$$

where $\Delta R \in \{-R_\star,\ R_\star\}$, the negative sign corresponds to the region toward BH. The spin factor k is (Alexander & Kumar 2001)

$$k = \begin{cases} 1 & \text{non spin up (no change in angular velocity)} \\ 3 & \text{spin up to break up angular velocity} \end{cases}$$

The maximum distance from the center of star to the point where the debris is bound to the black hole at the moment of disruption is obtained by setting $E_d = 0$ and is given by

$$R_l(\bar{e},\ \ell,\ M_\bullet,\ m) = \frac{r_p^2 \bar{e}}{2k\, r_t}. \tag{17}$$

The time taken for the most tightly bound debris to return its pericenter after disruption is given by

$$t_m(\bar{e},\ \ell,\ M_\bullet,\ m) = \frac{2\pi GM_\bullet}{(2E_d)^{3/2}}. \tag{18}$$

Accretion rate

The infall mass accretion rate at time t after disruption for the debris following Keplerian orbits is given by (Phinney 1989)

$$\frac{\mathrm{d}M}{\mathrm{d}t} = \frac{\mathrm{d}M}{\mathrm{d}E_d}\frac{\mathrm{d}E_d}{\mathrm{d}a}\frac{\mathrm{d}a}{\mathrm{d}t} = \frac{1}{3}(2\pi G M_\bullet)^{\frac{2}{3}}\frac{\mathrm{d}M}{\mathrm{d}E_d}t^{-\frac{5}{3}} \tag{19}$$

In terms of dimensionless variables
$x_l = R_l/R_\star$, $x = \Delta R/R_\star$,
$\mu = M/M_\star$ and $\tau = t/t_m$,
$\varepsilon = E_d/E_{dm}$ where
$E_{dm} = E_d(\bar{e},\ \ell,\ M_\bullet,\ m,\ -R_\star)$,

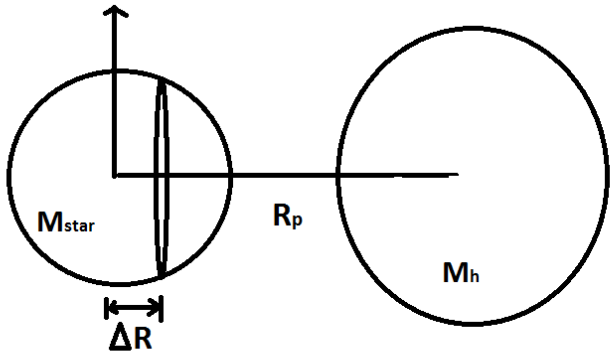

Figure: Schematic view of the geometry of the system.

The dimensionless quantities in Lodato et al. (2009) gets modified to

$$\varepsilon = \frac{x_l - x}{x_l + 1}, \qquad x = x_l - \tau^{-2/3}(1 + x_l) \tag{20}$$

$$\frac{\mathrm{d}\mu}{\mathrm{d}\varepsilon} = (1 + x_l)\frac{\mathrm{d}\mu}{\mathrm{d}x}, \qquad \frac{\mathrm{d}\mu}{\mathrm{d}\tau} = \frac{2}{3}\frac{\mathrm{d}\mu}{\mathrm{d}\varepsilon}\tau^{\frac{-5}{3}} \tag{21}$$

Accretion rate

The term $\mathrm{d}\mu/\mathrm{d}x$ is given by

$$\frac{\mathrm{d}\mu}{\mathrm{d}x} = \frac{3}{2} b \int_x^1 \theta^u(x') x' \, \mathrm{d}x' \tag{22}$$

where b is the ratio of central density ρ_c to mean density $\overline{\rho_\star} = 3M_\star/4\pi R_\star^3$ and θ is the solution of Lane-Emden equation for the given polytrope u related to the density by $\rho = \rho_c \theta^u$.

Thus the accretion rate is given by

$$\boxed{\frac{\mathrm{d}M}{\mathrm{d}t}(\bar{e},\ \ell,\ M_\bullet,\ m,\ t) = \frac{M_\star}{t_m}\frac{\mathrm{d}\mu}{\mathrm{d}\tau}}$$

The adiabatic index is taken to be

$$\Gamma = 1 + \frac{1}{u} = \frac{5}{3}$$

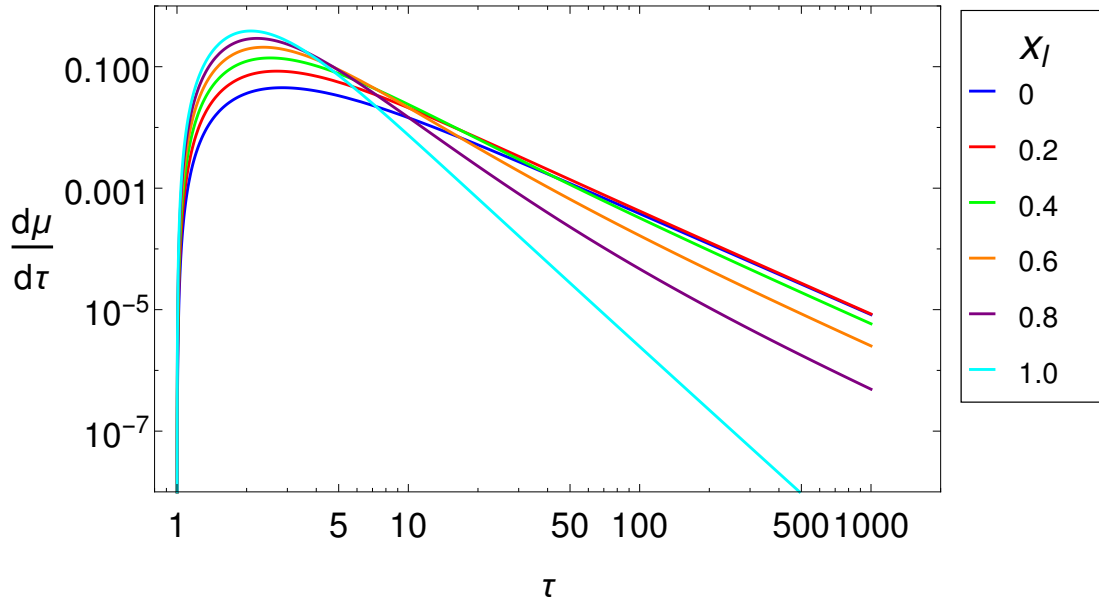

Figure: Dimensionless mass accretion rate

Disk formation: timescales

The important timescales are

- Accretion timescale t_a
- Ring timescale t_r
- Radiation timescale t_R
- Viscous timescale t_v

Accretion timescale

We have approximated $\mathrm{d}\mu/\mathrm{d}x \simeq 1.192e^{-4.321x^2}$ and the total mass consumed in dimensionless time $\tau_a = t_a/t_m$ is given by

$$\Delta\mu = \int_1^{\tau_a} \frac{\mathrm{d}\mu}{\mathrm{d}\tau}\,\mathrm{d}\tau \tag{23}$$

If f_r is the fraction of debris bound to the black hole, then in time τ_a, the mass accreted by the black hole is $\sim 0.99 f_r$. Then, the accretion timescale t_a is given by

$$t_a(\bar{e},\ \ell,\ M_\bullet,\ m) = t_m \left(\frac{1 + x_l}{x_l + \frac{1}{2.0787}\mathrm{Erf}^{-1}[0.997 - 1.962 f_r]} \right)^{\frac{3}{2}} \tag{24}$$

where

$$f_r \equiv f_r(\bar{e},\ \ell,\ M_\bullet,\ m) = \int_{-1}^{x_l} \frac{\mathrm{d}\mu}{\mathrm{d}x}\,\mathrm{d}x \tag{25}$$

Disk formation: timescales

Ring timescale

The energy gradient between the bound debris will fill out a ring and the initial spatial distance between the bound debris will determine the ring formation timescale t_r.

$$t_r = \frac{2\pi}{\Delta\Omega}; \quad \Omega = \frac{(2E)^{\frac{3}{2}}}{GM_\bullet}; \quad \Delta\Omega \propto E^{1/2}\Delta E;$$

where

$$\Delta E(\bar{e},\ \ell,\ M_\bullet,\ m) = \frac{2kGM_\bullet}{r_p^2}(\mathrm{Min}[R_l,\ R_\star] + R_\star)$$

Then, t_r is given by

$$t_r(\bar{e},\ \ell,\ M_\bullet,\ m) = \frac{\pi}{3\sqrt{2}k}\frac{r_p^2}{\bar{e}^{1/2}E_m^{1/2}}(R_\star + \mathrm{Min}[R_l,\ R_\star])^{-1} \tag{26}$$

The ratio of ring to accretion timescale is $\mathcal{T}_r$ given by

$$\mathcal{T}_r(\bar{e},\ \ell,\ M_\bullet,\ m) = \frac{1}{3\sqrt{2}}\frac{x_l}{1+\mathrm{Min}[1,\ x_l]}\left(\frac{x_l + \frac{1}{2.0787}\mathrm{Erf}^{-1}[0.997 - 1.962f_r]}{x_l}\right)^{\frac{3}{2}} \tag{27}$$

Disk formation: timescales

An accretion disk is formed if $\mathcal{T}_r < 1$.

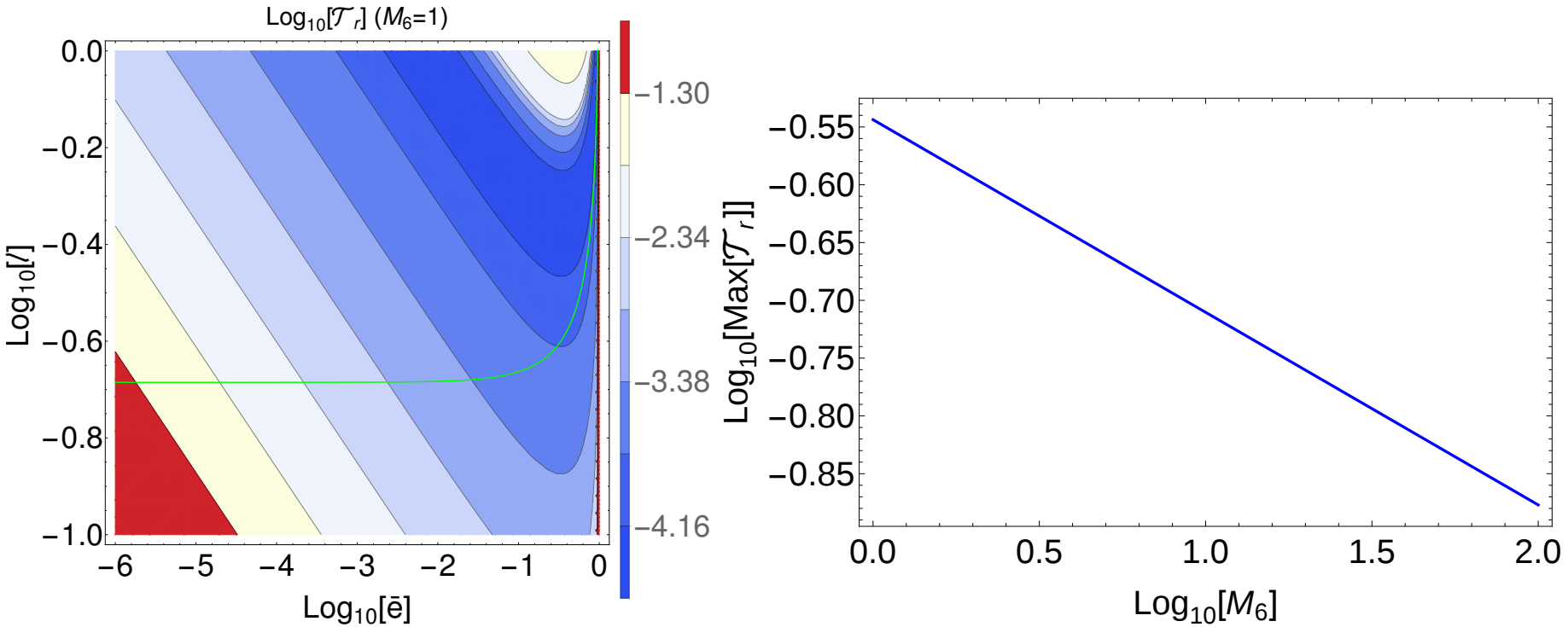

Figure: (Left) shows contour plot of the ratio $\mathcal{T}_r(\bar{e},\ \ell,\ M_6,\ m)$ for $M_6 = 1$ and $m = 1$. The green line correspond to $r_p = R_s$. For $r_p > R_S$ which lies above green line, $\mathcal{T}_r(\bar{e},\ \ell) < 1$ and thus an accretion disk is formed. (Right) shows the Max$[\mathcal{T}_r(\bar{e},\ \ell)]$ as a function of M_6 obtained in the range $10^{-6} \leq \bar{e} \leq 1$ and $0 \leq \ell \leq 1$.

Disk formation: timescales

The radiation timescale of the disk is given by

$$t_R(\bar{e},\ \ell,\ M_\bullet,\ m) = \frac{f_r M_\star c^2}{\eta \dot{M}\ c^2} \tag{28}$$

where c is the light speed, $\dot{M}$ is the accretion rate and η is the radiative efficiency of the disk. The viscous timescale t_v of the disk formed is given by (Strubbe & Quataert 2009)

$$t_v = \int_{r_{in}}^{r_c} \frac{1}{V_r}\,\mathrm{d}r; \qquad V_r = -\frac{3}{2}\frac{\nu}{r}\frac{1}{f} \tag{29}$$

where V_r is the radial inflow velocity of matter in disk, r_{in} is the inner radius of disk, $r_c = 2r_p(1 - r_p\bar{e}/r_t)$ where r_c is the circularization radius and $f = 1 - \sqrt{\frac{r_{in}}{r}}$ and ν is the viscosity of the medium given by $\nu = \alpha c_s H$. The parameter α is taken to be 0.1 and $c_s = H\sqrt{GM_\bullet/r^3}$ where H is disk scale height given by

$$\frac{H}{r}(\bar{e},\ \ell,\ M_\bullet,\ m,\ r) = \frac{3}{4} f \left(\frac{\dot{M}}{\eta \dot{M}_E}\right)\left(\frac{r}{R_s}\right)^{-1}\left\{\frac{1}{2} + \left\{\frac{1}{4} + \frac{3f}{2}\left(\frac{\dot{M}}{\eta \dot{M}_E}\right)^2\left(\frac{r}{R_s}\right)^{-2}\right\}^{\frac{1}{2}}\right\}^{-1} \tag{30}$$

where $\dot{M}_E$ is Eddington mass accretion rate.

Disk formation: timescales

The viscous timescale is given by

$$t_v(\bar{e},\ \ell,\ M_\bullet,\ m) = \frac{2}{3\alpha}\frac{1}{\sqrt{GM_\bullet}}\int_{r_{in}}^{r_c(\bar{e},\ \ell,\ M_\bullet,\ m)}\left(\frac{H(\bar{e},\ \ell,\ M_\bullet,\ m,\ r)}{r}\right)^{-2}\sqrt{r}f\,\mathrm{d}r \qquad (31)$$

Thus, $\mathcal{T}_v = t_v/t_R$

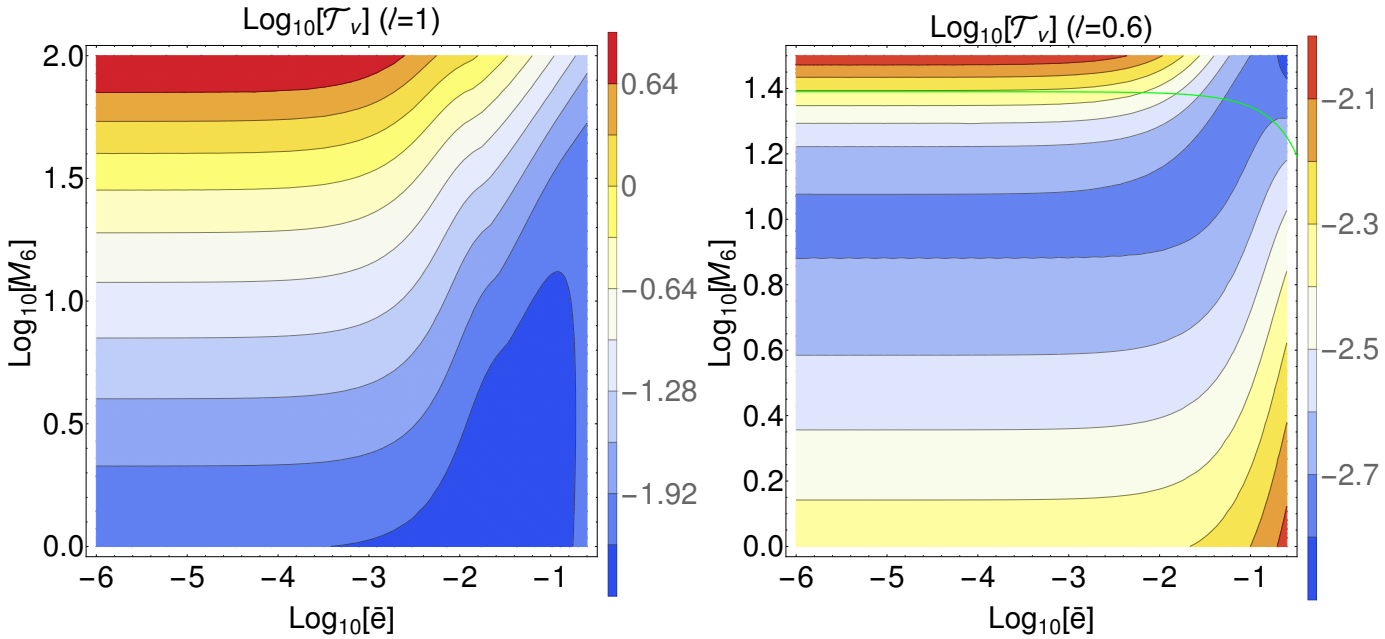

Figure: The contour plot of $\mathcal{T}_v(\bar{e},\ \ell,\ M_\bullet,\ m)$ is shown for $\ell = 1$ (top) and $\ell = 0.6$ (bottom) for $m = 1$. The green line corresponds to $r_p = R_s$. For $M_6 \leq$ 31.6, the accretion disk formed is a slim disk. For higher mass SMBHs, a thin disk forms from the disrupted debris of a star on low energy orbit and $\ell \sim 1$ and a thick disk for a star on high energy orbit.

Accretion rate Vs Eddington rate: Critical black hole mass

The Eddington rate is given by

$$\dot{M}_E = \frac{4\pi G M_\bullet}{\eta \kappa c} \qquad (32)$$

where $\eta = 0.1$ and $\kappa = 0.04\ \mathrm{m^2 Kg^{-1}}$. Numerically equated $\dot{M}_p = \dot{M}_E$ and obtained critical black hole mass M_c.

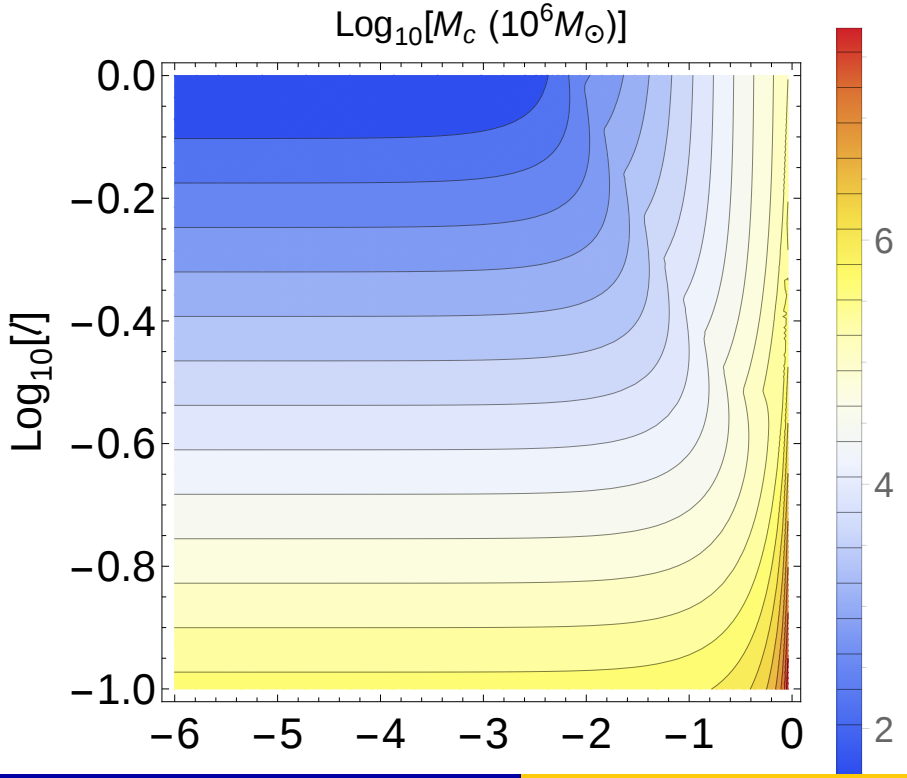

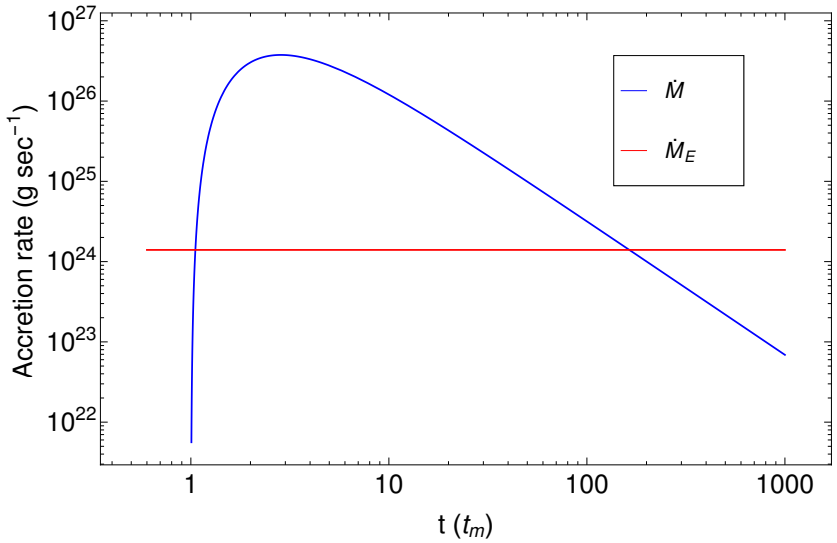

Figure: Parabolic orbit $\bar{e} = 10^{-6}$, $\ell = 1$ and $M_6 = 1$ such that $t_m = 2.78$ days.

A contour plot of $M_c(\bar{e},\ \ell,\ m)$ is shown for the disruption of a star of solar mass. The peak $\dot{M}$ increases with a decrease in ℓ and increase in $\bar{e}$ and thus, the M_c increases with $\bar{e}$ and decreases with ℓ

Accretion disk: Super Eddington phase

In Super Eddington phase,

- Accretion rate $\dot{M} \geq \dot{M}_E$.
- Disk is radiatively inefficient.
- Radiation pressure dominated.
- Energy flows through advection.
- Mass loss due to outflowing wind.

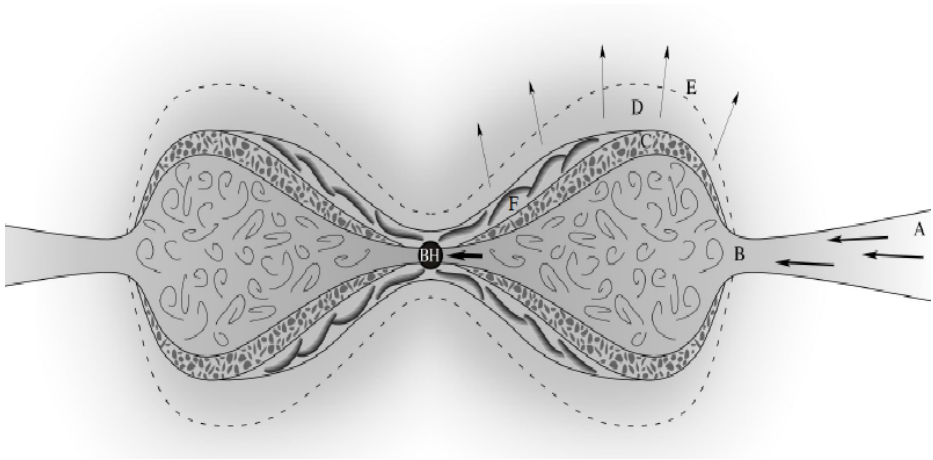

Figure: Slim disk model. Different region are: (A) Sub Eddington thin disc. (B) Radiation pressure dominated region. (C) Porus layer forms at less dense region above convection layer. (D) Thin porus layer, wind is accelerated.

Source: Dotan & Shaviv (2011)

Super Eddington phase

We approximate the outflow's geometry as spherical with density profile

$$\rho(r) \sim \frac{\dot{M}_{out}}{4\pi r^2 v_w}$$

The radiation temperature at the base of the wind $T_L = T(r_L)$ where $r_L(\bar{e},\ \ell,\ M_\bullet,\ m) = 2r_p(1 - r_p\bar{e}/r_t)$

$$aT_L^4 \sim \frac{1}{2}\rho(r_L)v_w^2$$

Radius of the photosphere is given by

$$r_{ph}(\bar{e},\ \ell,\ M_\bullet,\ m,\ t) = \frac{\dot{M}_{out}\kappa}{4\pi v_w}$$

where $\dot{M}_{out} = f_{out}\dot{M}$, $v_w = f_v\sqrt{GM_\bullet/r_L}$ is the velocity of out flowing wind and κ is opacity due to electron scattering.
The outflow wind is assumed to expand adiabatically such that $\rho(r) \propto T^3$, thus photosphere temperature is given by

$$T_{ph}(\bar{e},\ \ell,\ M_\bullet,\ m,\ t) = (4\pi)^{\frac{5}{12}}\left(\frac{1}{2a}\right)^{\frac{1}{4}}\kappa^{-\frac{2}{3}}f_{out}^{-\frac{5}{12}}f_v^{\frac{11}{12}}\dot{M}^{-\frac{5}{12}}r_L^{-\frac{7}{24}}(GM_\bullet)^{\frac{11}{24}}. \qquad (33)$$

Super Eddington phase

The fraction of outflowing mass f_{out} is given by

$$f_{out} = \frac{2}{\pi} \arctan \left[\frac{1}{4.5} \left(\frac{\dot{M}}{\dot{M}_E} - 1 \right) \right].$$

Thus, the luminosity is given by

$$L_\nu^{out}(\bar{e},\ \ell,\ M_\bullet,\ m,\ t) = 4\pi r_{ph}^2 B_\nu(T_{ph})$$

Since disk is radiatively inefficient, the temperature of the disk is given by

$$\sigma_{SB} T_e^4(\bar{e},\ \ell,\ M_\bullet,\ m,\ r,\ t) = 8.54 \times 10^{17} \frac{M_6^{-1} \left(\frac{\eta}{0.1}\right)^{-1} \left(\frac{r}{R_s}\right)^{-3} \left(\frac{\dot{M}}{\dot{M}_E}\right) f}{\frac{1}{2} + \left\{ \frac{1}{4} + \frac{3f}{2} \left(\frac{\dot{M}}{\eta \dot{M}_E}\right)^2 \left(\frac{r}{R_s}\right)^{-2} \right\}^{\frac{1}{2}}} \quad \mathrm{W\,m^{-2}}$$

Disk emission

For a sub Eddington disk, $\dot{M} < \dot{M}_E$ and thus the disk is considered to a thin disk with temperature profile

$$\sigma_{SB} T_e^4(\bar{e},\ \ell,\ M_\bullet,\ m, r,\ t) = 8.54 \times 10^{17} M_6^{-1} \left(\frac{\eta}{0.1}\right)^{-1} \left(\frac{r}{R_s}\right)^{-3} \left(\frac{\dot{M}}{\dot{M}_E}\right) f \quad \mathrm{W\,m^{-2}} \tag{34}$$

thus the disk luminosity is given by

$$L_\nu^{Disk}(\bar{e},\ \ell,\ M_\bullet,\ m,\ t) = \int_{r_{in}}^{r_c(\bar{e},\ \ell,\ M_\bullet,\ m)} B_\nu(T_e(\bar{e},\ \ell,\ M_\bullet,\ m, r,\ t)) 2\pi r\, \mathrm{d}r, \tag{35}$$

The total luminosity can be written as

$$L_\nu(\bar{e},\ \ell,\ M_\bullet,\ m,\ t) = \begin{cases} L_\nu^{Disk} + L_\nu^{out} & M_\bullet < M_c(\bar{e},\ \ell,\ m) \\ L_\nu^{Disk} & M_\bullet \geq M_c(\bar{e},\ \ell,\ m) \end{cases}$$

If ν_l and ν_h are the minimum and maximum frequency of the spectral band, then the luminosity of the emitted radiation in the given spectral band in the rest frame of the galaxy is given by

$$L_e(\bar{e},\ \ell,\ M_\bullet,\ m,\ z,\ t) = \int_{\nu_l(1+z)}^{\nu_h(1+z)} L_\nu(\bar{e},\ \ell,\ M_\bullet,\ m,\ t)\, \mathrm{d}\nu \tag{36}$$

Observed flux

The radiation emitted from the source is observed only if observed flux f_{obs} is higher than detectors sensitivity f_l.

$$f_l < f_{obs}(\bar{e},\ \ell,\ M_\bullet,\ m,\ z,\ t) = \frac{L_e(\bar{e},\ \ell,\ M_\bullet,\ m,\ z,\ t)}{4\pi d_L^2(z)} \tag{37}$$

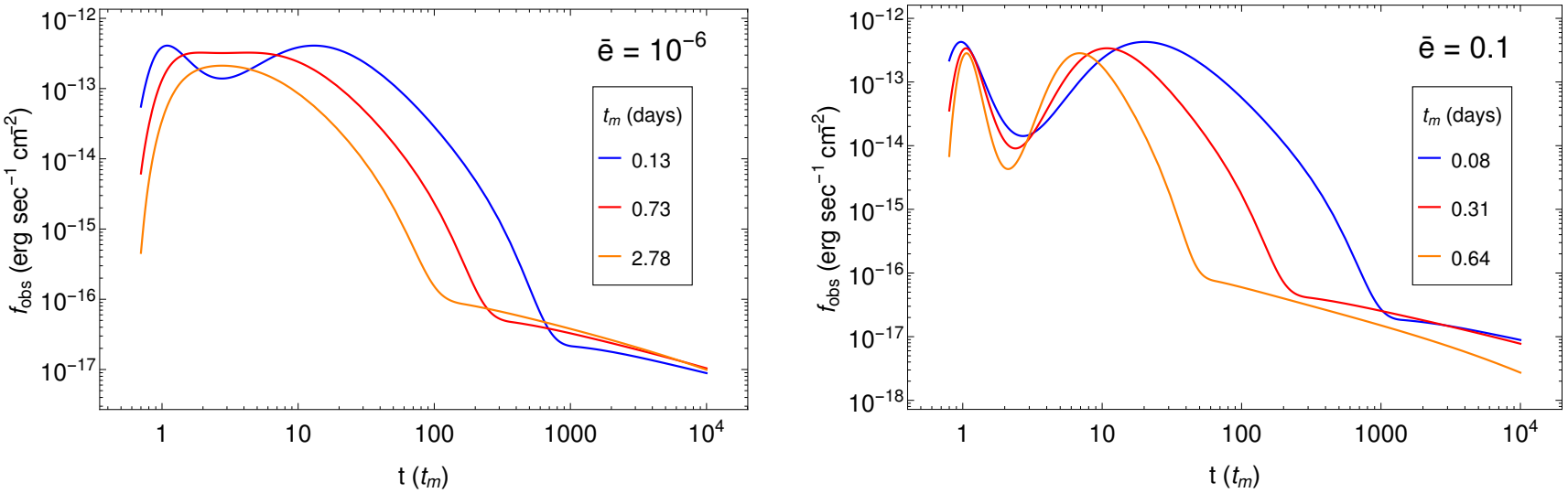

Figure: The observed flux f_{obs} (eqn (37)) in the optical g-band for $M_6 = 1$, $m = 1$, redshift $z = 0.1$ and ℓ= 0.6 (blue), 0.8 (red), 1.0 (orange). The peak flux decreases with ℓ and the light curve profile gets widened with decrease in ℓ. The initial dip in the flux is due to the out flowing wind. The t_m is time taken for the most tightly bound debris to return its pericenter after disruption.

Probability of detection

The eqn (37) is utilized to generate a digital signal $A(t)$ such that

$$A(t) = \begin{cases} 1 & \text{if eqn } (37) \text{ holds true} \\ \\ 0 & \text{if eqn } (37) \text{ does not hold true} \end{cases} \tag{38}$$

The width of the digital signal gives the duration of flare detection $\delta t_f(\bar{e},\ \ell,\ M_\bullet,\ m,\ z)$. If t_{cad} and t_{int} are cadence and integration time of the detector, then the probability of detection of an event is given by

$$P(\bar{e},\ \ell,\ M_\bullet,\ m,\ z) = \text{Min}\left[1,\ \frac{\delta t_f(\bar{e},\ \ell,\ M_\bullet,\ m,\ z)}{t_{cad} + t_{int}}\right] \tag{39}$$

Number density of non active galaxies

Quasar luminosity function [Hopkins et al. 2007]

$$\frac{\mathrm{d}\Psi}{\mathrm{d}\log L} = \frac{\Psi_*}{(\frac{L}{L_*})^{\gamma_1} + (\frac{L}{L_*})^{\gamma_2}}$$

where $\Psi_*, L_*, \gamma_1, \gamma_2$ are function of redshift.

According to the Soltan (1982) argument, if quasars were powered by accretion onto a SMBH, then such SMBH must exist in our local universe as “dead” quasars or non active galaxies.

Duty cycle is number of active galaxies to total number of galaxies [Chen & Wang 2007]

$$\delta(z) = 10^{-3}\left(\frac{z}{0.1}\right)^{2.5}$$

Number density of non active galaxies

Luminosity function of non active galaxies

$$\left(\frac{\mathrm{d}\Psi}{\mathrm{d}\log L}\right) = (1-\delta(z))\frac{\mathrm{d}\Psi}{\mathrm{d}\log L}$$

Black hole mass function of galaxies can be written as

$$\left(\frac{\mathrm{d}\Psi}{\mathrm{d}M_\bullet}\right) = (1-\delta(z))\frac{\mathrm{d}\Psi}{\mathrm{d}\log L}\left|\frac{\mathrm{d}\log L}{\mathrm{d}M_\bullet}\right|$$

The L is the luminosity of the quasars which is taken as

$$L = \eta L_E = \frac{\eta 4\pi G M_\bullet c}{\kappa}$$

where η is taken to be 0.1 , $\kappa = 0.4\mathrm{cm}^2\ \mathrm{g}^{-1}$ (Thompson opacity) , L_E are the efficiency, opacity of the medium and the Eddington luminosity.

Luminosity Distance

- Luminosity distance

$$d_L(z) = (1+z)\frac{c}{H_o}\int_0^z \frac{1}{((1+z')^3\Omega_m + \Omega_\Lambda)^{0.5}}\, dz'.$$

where $\Omega_m = 0.315, \Omega_\Lambda = 0.685, H_o = 67.3\ \mathrm{Km\ sec^{-1}\ Mpc^{-1}}$ [Planck collaboration 2013]

- Comoving volume

$$\mathrm{d}V_c = \omega d_H^3 \frac{J^2(z)}{E(z)}\mathrm{d}z,$$

where $\omega = 4\pi f_s, d_H = \frac{c}{H_o}, E(z) = ((1+z)^3\Omega_m + \Omega_\Lambda)^{0.5}$

$J(z) = \int_0^z \frac{1}{((1+z')^3\Omega_m+\Omega_\Lambda)^{0.5}}\, dz'.$

Detectable rates

The net detectable rates is given by

$$\dot{N}_D = \int_1^{100} \mathrm{d}M_6 \int_{0.8}^{150} \mathrm{d}m \int_{\bar{e}_h}^1 \mathrm{d}\bar{e} \int_0^1 \mathrm{d}\ell \int_0^{z_s} \mathrm{d}z \; \omega d_H^3 \left(\frac{\mathrm{d}\Psi}{\mathrm{d}M_\bullet}\right) \frac{\mathrm{d}^3\dot{N}_t}{\mathrm{d}\bar{e}\mathrm{d}\ell\mathrm{d}m}(\gamma, \bar{e}, \ell, M_\bullet, m) \frac{I^2(z)}{W(z)} P(\bar{e}, \ell, M_\bullet, m, z) \tag{40}$$

The occurrence rate of TDE is given by

$$\dot{N}_o = \int_1^{100} \mathrm{d}M_6 \int_{0.8}^{150} \mathrm{d}m \int_{\bar{e}_h}^1 \mathrm{d}\bar{e} \int_0^1 \mathrm{d}\ell \int_0^{z_s} \mathrm{d}z \quad \omega d_H^3 \left(\frac{\mathrm{d}\Psi}{\mathrm{d}M_6}\right) \frac{\mathrm{d}^3\dot{N}_t}{\mathrm{d}\bar{e}\mathrm{d}\ell\mathrm{d}m}(\gamma, \bar{e}, \ell, M_6, m) \frac{I^2(z)}{W(z)} \tag{41}$$

We define the detection efficiency of TDE for a detector to be

$$\Upsilon = \frac{\dot{N}_D}{\dot{N}_o} \tag{42}$$

The only free parameter in our estimate is γ and this is likely to vary from source to source. Not knowing the expected distribution of γ as a function of say redshift, we have calculated the error in our estimation of $\dot{N}_D$ by taking a fiduciary range in the observed median of $\gamma = 0.7 \pm 0.1$ and is shown in Table 1 along with the efficiency of the detections. The values of γ for which our predictions of $\dot{N}_D$ matches with the scaled up values in Van Velzan et al. (2011) are shown as γ_s in Table 1.

Detectable rates

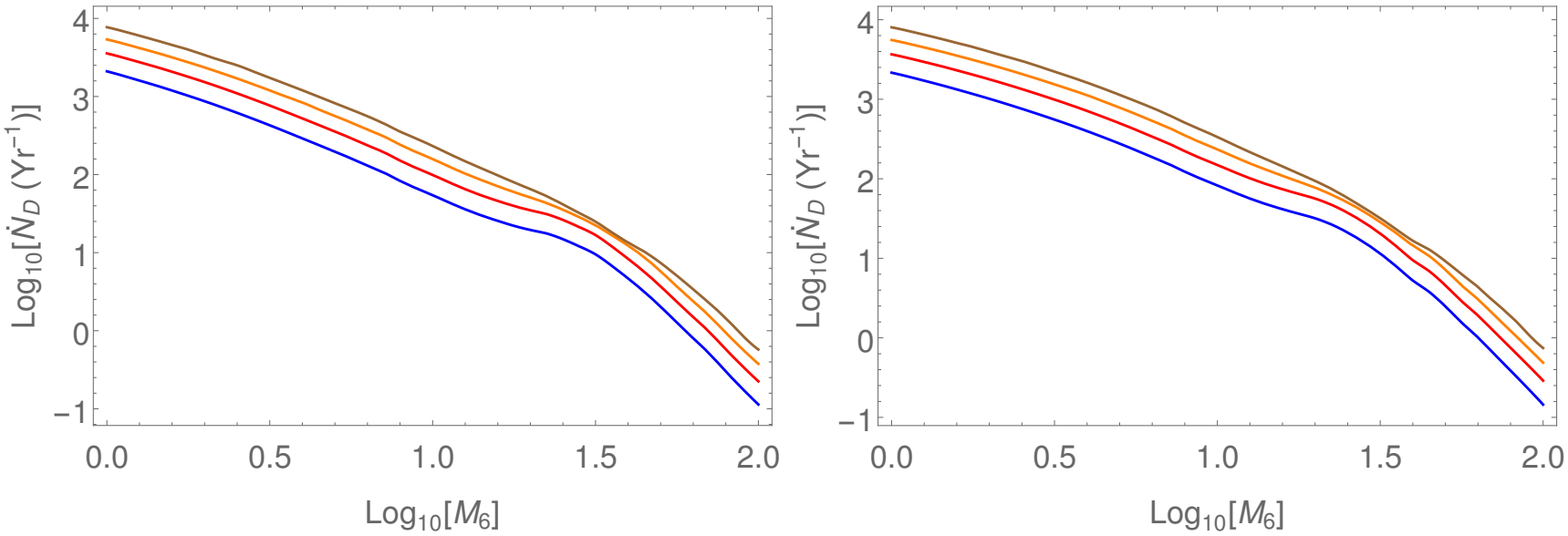

Figure: The detectable rate, $\dot{N}_D$, per M_6 for various γ for (a) LSST survey and (b) Pan-STARRS 3π survey. With increase in γ, the detectable rate increases due to increase in $\dot{N}_t$.

Detectable rates

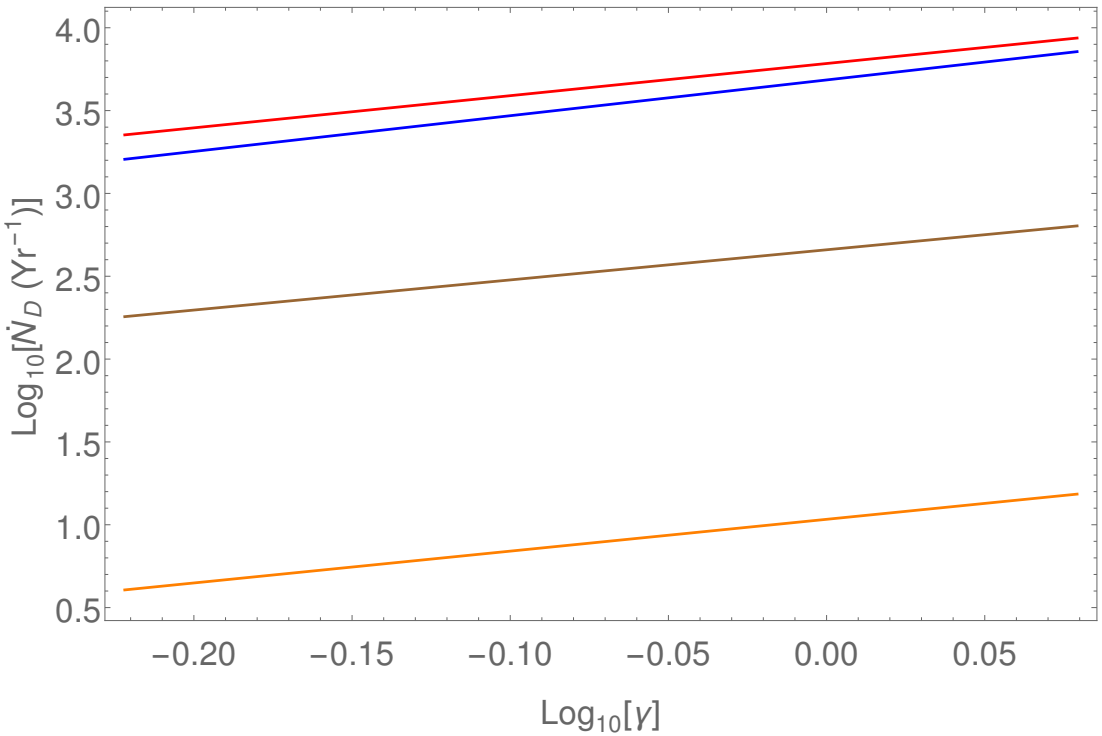

Figure: The detectable rate, $\dot{N}_D$, as a function of γ for LSST (blue), Pan-STARRS 3π (red), Pan-STARRS MDS (orange) and eROSITA (brown). It is seen that $\dot{N}_D \propto \gamma^{\Delta}$ where Δ is the slope given in Table 1.

Predicted rates for various surveys

Survey	Band	f_s	sensitivity $\mathrm{erg\ sec^{-1}\ cm^{-2}}$	t_{cad} (sec)	t_{int} (sec)	$\dot{N}_D\ (\mathrm{Yr}^{-1})^{\ddagger}$ $\gamma = 0.7 \pm 0.1$	γ_s^{+}	$\dot{N}_{obs}\ (\mathrm{Yr}^{-1})^{\dagger}$	$\Upsilon^{\times}$	Δ^{*}
LSST	Optical	0.5	1.15×10^{-15}	2.6×10^{5}	10	5003 ± 1421	0.63	4131	0.91	1.97
Pan-STARRS (MDS)	Optical	0.0012	1.8×10^{-15}	3.46×10^{5}	30	12.3 ± 3.5	0.77	15	0.92	1.98
Pan-STARRS 3π	Optical	0.75	8.73×10^{-16}	6.05×10^{5}	30	6337 ± 1800	0.48	3106	0.85	1.94
eROSITA	X-Ray	1	2.4×10^{-14}	1.58×10^{7}	1.6×10^{3}	679.5 ± 195	–	–	0.7	2.06

References & Notes: (1) LSST: Strubbe & Quataert (2009) & `http://www.lsst.org/lsst/overview/`

(2) Pan-STARRS (MDS): Medium Deep survey: Van Velzan et al. (2011)

(3) Pan-STARRS 3π: Strubbe & Quataert (2009) & `http://pan-starrs.ifa.hawaii.edu/public/`

(4) eROSITA (SRG): Khabhibullin et al. (2009) & `http://www.mpe.mpg.de/eROSITA`

$\ddagger$ Our predicted values, $\dagger$ Results from Van Velzan et al. (2011), $*$ Detectable rate $\dot{N}_D \propto \gamma^{\Delta}$

$^{+}\dot{N}_D(\gamma_s) = \dot{N}_D$ estimated by Van Velzan et al. (2011), $\times$ detection efficiency of the detector

$^{\triangle}$ Sensitivity: LSST, Pan-STARRS 3π and Pan-STARRS MDS in optical g band and eROSITA in soft x-ray band.

t_{cad} and t_{int} are the cadence and integration time of the detector.

Table: Surveys and predicted rates

Conclusions

The star's initial orbital parameters E and J have significant effects on both stellar and accretion dynamics. We have seen that the effect of J which has not been included previously, plays a crucial role in constructing the shape of light curve profiles.

- For $M_6 > 10$, $\dot{N}_t \propto M_6^{-\beta}$ where $\beta = 0.3 \pm 0.01$ and $\dot{N}_t \approx \gamma^{2\cdot}$. The galaxy averaged and γ averaged $\dot{N}_t$ integrated over the range $0.6 \leq \gamma \leq 1.2$ is $\sim 1.3 \times 10^{-4}$ Yr^{-1}.
- The applicable ranges of dimensionless energy $\bar{e}$ and angular momentum ℓ are given by $\{\bar{e}_h < \bar{e} < 1, 0 < \ell < 1\}$ where $\bar{e}_h = r_t/r_h$.
- The peak accretion rate increases with $x_l = R_l/R_\star$. The decline to later $t^{-5/3}$ law is steeper if the energy of the initial orbit is higher.
- We have found that Max[$\mathcal{T}_r(\ 10^{-6} \leq \bar{e} \leq 1,\ 0 \leq \ell \leq 1, 1 \leq M_6 \leq 100)$]$< 1$ which implies that the debris will form an accretion disk.
- The ratio $\mathcal{T}_v < 1$ for $M_6 \leq 31.6$ which implies that the accretion disk formed is a slim disk. The higher mass SMBHs forms a thin disk from the disrupted debris of a star on low energy orbit and $\ell \sim 1$ and a thick disk for a star on a high energy orbit.

Conclusions

- The peak of observed flux decreases with ℓ. The decline of light curve profile to later stage gets steeper with increase in ℓ.
- Our results are in reasonable agreement with the scaled up values from the SDSS observations Van Velzan et al. (2011) for $\gamma = 0.7$. The Υ is lowest for the eROSITA mission due to high cadence of half year and is highest for Pan-STARRS MDS due to very high sensitivity. The $\dot{N}_D \propto \gamma^{\Delta}$ where $\Delta \sim 1.95$ in optical band.

Survey	$\dot{N}_D\ (\mathrm{Yr}^{-1})$ $\gamma = 0.7 \pm 0.1$	γ_s	$\dot{N}_{obs}\ (\mathrm{Yr}^{-1})$	Υ	Δ
LSST	5003 ± 1421	0.63	4131	0.91	1.97
Pan-STARRS (MDS)	12.3 ± 3.5	0.77	15	0.92	1.98
Pan-STARRS 3π	6337 ± 1800	0.48	3106	0.85	1.94
eROSITA	679.5 ± 195	–	–	0.7	2.06

Classical Hydromagnetic winds theory

- A complete solution should provide the run of density, velocity and energy along the stream lines. The usual simplification of axisymmetry is made and a steady state is assumed.
- A distinction is made between the force-free models where the inertia is ignored, and those that include inertial forces in the treatment.
- The Blandford & Payne (1982) model involves a further simplification, namely that of self-similarity, i.e., the properties of the solution are independent of the location, arising from an expectation that the extraction of angular momentum ($\propto r^{1/2}$) scales similarly in radius as magnetic torque ($\sim \psi^2/r \sim B^2 r^3$) which demands that the magnetic field scale as $r^{-5/4}$.
- Solutions to observables such as the terminal speed of the jet, the luminosity or the thrust in the jet

Properties of steady axisymmetric flow

The basic conservation laws were worked out by Chandrasekhar (1956) and redone by Mestel (1961) and applied to rotating stars; an algebraic variation of the latter calculation follows.

$$\nabla \times (\mathbf{v} \times \mathbf{B}) = 0, \tag{43}$$

where by axisymmetry one can write the velocity and magnetic fields as

$$\mathbf{B} = \mathbf{B}_p + \mathbf{B}_\phi \qquad \text{and} \qquad \mathbf{v} = \mathbf{v}_p + \mathbf{v}_\phi, \tag{44}$$

in the usual cylindrical coordinate system; the toroidal velocity is $\mathbf{v}_\phi = \omega r$. Since the toroidal term, $\mathbf{v}_p \times \mathbf{B}_p$, cannot be a gradient of a potential, the poloidal part of the flux freezing condition (43) implies that

$$\mathbf{v}_p = \frac{\kappa(\psi)}{4\pi\rho}\mathbf{B}_p, \tag{45}$$

where κ is a constant on each magnetic surface.

Properties of steady axisymmetric flow

$$\nabla \times (\mathbf{v}_\phi \times \mathbf{B}_p + \mathbf{v}_p \times \mathbf{B}_\phi) = 0$$

$$(\mathbf{B}_p \cdot \nabla)\mathbf{v}_\phi - (\mathbf{v}_\phi \cdot \nabla)\mathbf{B}_p - (\mathbf{B}_p \cdot \nabla)(\frac{\kappa(\psi)}{4\pi\rho}\mathbf{B}_\phi) + (\mathbf{B}_\phi \cdot \nabla)(\frac{\kappa(\psi)}{4\pi\rho}\mathbf{B}_p) = 0$$

$$(\mathbf{B}_p \cdot \nabla - \frac{B_r}{r})(\frac{\kappa(\psi)}{4\pi\rho}\mathbf{B}_\phi - \mathbf{v}_\phi) = 0$$

$$(\mathbf{B}_p \cdot \nabla)(\frac{\kappa(\psi)}{4\pi\rho r}\mathbf{B}_\phi - \boldsymbol{\omega}) = 0$$

$$\frac{\kappa(\psi)}{4\pi\rho r}B_\phi - \omega = \omega_f(\psi) \tag{46}$$

where $\omega_f(\psi)$ is the angular speed of the magnetic surface. Next, we write the Euler's equation for a magnetized, warm gas in a gravitational potential, φ_g, as

$$\nabla\left[(v_p^2 + \omega^2 r^2)/2 + \varphi_g + H\right] = \frac{1}{4\pi\rho}(\nabla \times \mathbf{B}) \times \mathbf{B} - (\nabla \times \mathbf{v}) \times \mathbf{v}, \tag{47}$$

where H is the specific enthalpy of the gas.

Properties of steady axisymmetric flow

The toroidal component of this equation, to which the gradient term does not contribute, is

$$\begin{aligned}
(\mathbf{B}_p \times \nabla \times \mathbf{B}_\phi)/4\pi\rho &= \mathbf{v}_p \times \nabla \times \mathbf{v}_\phi \\
\nabla \times \mathbf{B}_\phi - \kappa(\psi)\nabla \times \mathbf{v}_\phi &\propto \mathbf{B}_p \\
\hat{P}(rB_\phi) - \kappa(\psi)\hat{P}(r^2\omega) &\propto \hat{P}(\psi) \\
r^2\omega - \frac{rB_\phi}{\kappa(\psi)} &= \ell(\psi) \equiv \omega_f(\psi) r_A^2(\psi), \qquad (48)
\end{aligned}$$

and the integral of motion that results is the conservation of total angular momentum of the system, $\ell(\psi)$, with its lever arm defined as the Alfvén radius, r_A, containing both the gas and field contributions.

Properties of steady axisymmetric flow

The flow energetics involving the Bernoulli and Grad-Shafranov equations (to be derived below) were used to describe the plasma confinement in tokomaks (e.g. Shafranov 1965) and in the vicinity of pulsars (e.g. Michel 1973). Here we shall present a slightly modified treatment of Pelletier & Pudritz (1992). The Bernoulli equation (see for e.g., Chandrasekhar 1961) can be written as

$$1/2(v_p^2 + \omega^2 r^2) + \varphi_g + H + \omega_f(\omega_f r_A^2 - \omega r^2) = E(\psi), \tag{49}$$

where the last term on the left is the work done by the field on the gas and is given by (48), while the specific energy, $E(\psi)$, is constant along streamlines. This may also be obtained by taking the component of (47) along the magnetic surface. It can be seen from the Bernoulli equation that the terminal speed of the gas will be

$$v_\infty(\psi) \sim \omega_f r_A, \tag{50}$$

if gravity is neglected at large distances from the source. Taking the gradient of (49)

$$\nabla E = d_\psi E \nabla\psi = \frac{1}{4\pi\rho}(\nabla \times \mathbf{B}) \times \mathbf{B} - (\nabla \times \mathbf{v}) \times \mathbf{v} + \nabla[\omega_f(\omega_f r_A^2 - \omega r^2)], \tag{51}$$

we find it is perpendicular to the magnetic surface.

Properties of steady axisymmetric flow

The various terms of the RHS are

$$(\nabla \times \mathbf{v}_\phi) \times \mathbf{v}_\phi = \hat{P}(r\omega) \times r\omega\hat{\phi} = -\omega\nabla(r^2\omega), \tag{52}$$

$$(\nabla \times \mathbf{B}_p) \times \mathbf{B}_p = \mathbf{B}_p \times (\hat{\phi}\frac{\Lambda\psi}{r}) = -\frac{1}{r^2}(\nabla\psi)(\Lambda\psi), \tag{53}$$

$$\begin{aligned}(\nabla \times \mathbf{v}_p) \times \mathbf{v}_p &= (\frac{\kappa}{4\pi\rho})^2[-\frac{1}{r^2}\nabla\psi\Lambda\psi] + \frac{\kappa}{4\pi\rho}B_p^2\nabla_p(\frac{\kappa}{4\pi\rho}) \\ &= \frac{\nabla\psi}{4\pi\rho r^2}\left[-(\frac{\kappa}{4\pi\rho})^2\Lambda\psi + \frac{1}{2}\nabla\psi\cdot(\frac{\kappa}{4\pi\rho})^2\right] \\ &= \frac{\nabla\psi}{4\pi r^2}[\frac{\rho_A}{\rho^2}\Lambda\psi + \frac{1}{2}\nabla(\frac{\rho_A}{\rho^2})\cdot\nabla\psi] \end{aligned} \tag{54}$$

and the hoop stress

$$(\nabla \times \mathbf{B}_\phi) \times \mathbf{B}_\phi = \hat{P}(rB_\phi) \times B_\phi\hat{\phi} = -\frac{1}{2r^2}\nabla(rB_\phi)^2. \tag{55}$$

Properties of steady axisymmetric flow

The final term in (51) works out to be

$$\nabla(\omega_f^2 r^2 \rho g/\rho_A) + \nabla(\omega_f^2 r_A^2), \tag{56}$$

where $\rho_A(\psi) \equiv \kappa^2/4\pi$ is the density at the Alfvén point (a ring on the magnetic surface where the poloidal velocity reaches Alfvén speed) and

$$g = \frac{\omega_f - \omega}{\omega_f} = \frac{r_A^2 - r^2}{r^2} \frac{\rho_A}{\rho - \rho_A}, \tag{57}$$

measures the angular velocity of the gas with respect to the fields; so that $0 < g < 1$ as the gas asymptotically loses its angular momentum to the fields.

Properties of steady axisymmetric flow

Using the above results it can be shown that

$$\omega_f r_A^2 - \omega r^2 = \omega_f r^2 g\rho/\rho_A. \tag{58}$$

$$-\frac{\nabla(rB_\phi)^2}{8\pi r^2} - g\omega_f \nabla(\omega r^2) = g\omega_f[-\frac{g\omega_f r^2}{\rho_A^2}\partial_\psi \rho_A - \nabla(\omega r_A^2)]\nabla\psi. \tag{59}$$

The last two terms along with the hoop stress provide the effects of collimation and hence, after collecting all terms, the Grad-Shafranov equation can written as

$$\frac{\rho_A - \rho}{\rho}\Lambda\psi + \frac{1}{2}\rho\nabla\psi\cdot\nabla(\frac{\rho_A}{\rho^2}) = 4\pi\rho r^2[d_\psi E + c(\psi, g; r)], \tag{60}$$

where, after some additional effort, the collimation term is found to be

$$c(\psi, g; r) = g\omega_f[d_\psi(\omega_f r_A^2) + g\omega_f r^2\frac{\rho}{2\rho_A^2}d_\psi\rho_A] + (1-g)\omega_f r^2 d_\psi(\omega_f) - d_\psi(\omega_f^2 r_A^2). \tag{61}$$

Properties of steady axisymmetric flow

The Grad-Shafranov equation also describes the decollimating effects of the centrifugal motion pushing against the magnetic surface. The full set of MHD wind equations (Bernoulli and the Grad-Shafranov) given above, are written in a general form including gravity, internal energy of the gas, field energy, and rotation, and contain the two functions $\psi(r, z)$ and $\rho(r, z)$, and four invariant functionals of ψ, namely, ρ_A, r_A, ω_f and E.

Critical surfaces

In the more general case of a magnetized adiabatic gas, it is found that there are three modes of propagation: Alfvén, fast and slow MHD waves, and their speeds depend on the direction of the wave, **k**, with respect to that of the uniform magnetic field, **n**. Alfvén waves are disturbances that are mutually perpendicular to the direction of their propagation and the magnetic field; the motion of the field line resembles that of a string plucked in $\mathbf{n} \times \mathbf{k}$ direction. If $\cos\theta \equiv \mathbf{n} \cdot \mathbf{k}$, the speed of the transverse Alfvén wave is

$$v_a = \left(\frac{B^2}{4\pi\rho}\right)^{1/2} \cos\theta \equiv v_A \cos\theta. \tag{62}$$

The other two waves are magnetosonic waves which have disturbances in the plane of **n** and **k**; they may not be just distortions of the field line, but also could represent compressions and rarefactions of the gas and the field. The restoring force is not merely magnetic tension, as in the plucked string analogy of the Alfvén wave, but in addition, a combination of magnetic and gas pressures.

Jets: Theoretical Motivation

1. GR numerical simulations (e.g. Koide et al. 1999; Gammie et al. 2003; McKinney 2006) with the Poynting flux in the inner jet due to magnetic field lines threading the disk or the ergosphere of a rotating black hole (Blandford & Znajek 1977) to ($r \sim 10^4 r_g$) in order to study the bulk Lorentz factor, jet opening angle, magnetic field strength and overall energetics.
2. For radiation pressure dominated models, there is a combination of the centrifugal force and the radiation pressure from the disk (Cao 2012).
3. Emission in AGN such as blazars from radio to optical to Gamma-rays (e.g. Abdo et al. 2011) and can be inferred in many cases to arise from the jet.

Rotational Energy Budget

1. Several models rely on extracting the rotational energy of the black hole that is provided by the budget of the difference between the black hole mass and the irreducible mass, $m - m_i$ where $m_i = \sqrt{mr_+/2}$
2. This implies that about a fraction of 0.29 of the mass can be extracted in principle.
3. The irreducible mass is a consequence of the law of black hole entropy via the area theorem ($A = 8\pi mr_+$) and even the GRB phenomenon has been sought to be explained using this budget.
4. There is another class of models that rely on the jet being powered by an MHD accretion disk based on the generic bead on a wire model.

Jet Power and Torque

We adopt the flexible paradigm that the jets are either powered totally by black hole spin, essentially by the Blandford-Znajek (1977; BZ) process or also partially from a magnetized accretion disk, as in the hybrid model of Meier (1999; 2001). The jet powers in these two cases can be written as (McDonald & Thorne 1982; Meier 1999)

$$\mathcal{L}_{\rm jet} = \begin{cases} \mathcal{L}_{\rm BZ} = & \frac{1}{32}\omega_F^2 B_\perp^2 R_H^2 j^2 c \quad \text{BZ process} \\ \\ \mathcal{L}_{\rm H} = & \frac{1}{32c}(B_\phi R_{ms}^2 \Omega)^2 \quad \text{Hybrid process} \end{cases}$$

$R_H = \left(r(j)m \equiv 1 + (1-j^2)^{1/2}\right) GM_\bullet/c^2$ is the radius of the event horizon of the BH, where $m \equiv GM_\bullet/c^2$, and $j = a/m$ is the dimensionless angular momentum of the BH; for the second expression.

Black hole Electrodynamics

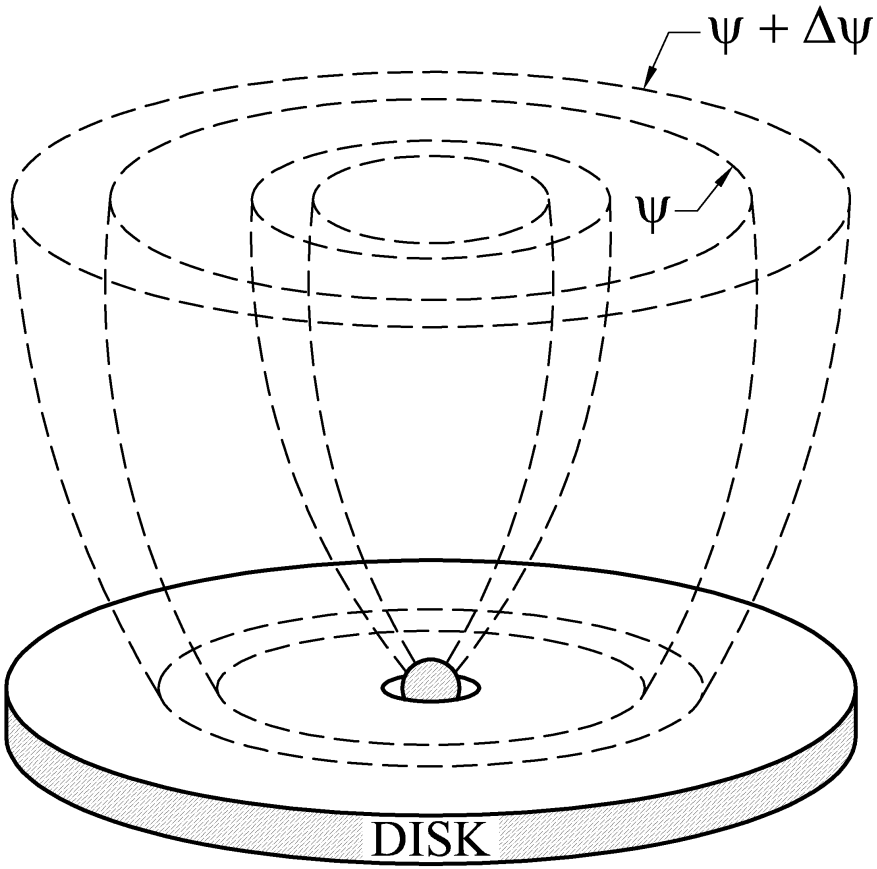

Figure: The BH rotational energy is lost by the BZ process and by Hybrid process

Black hole Electrodynamics

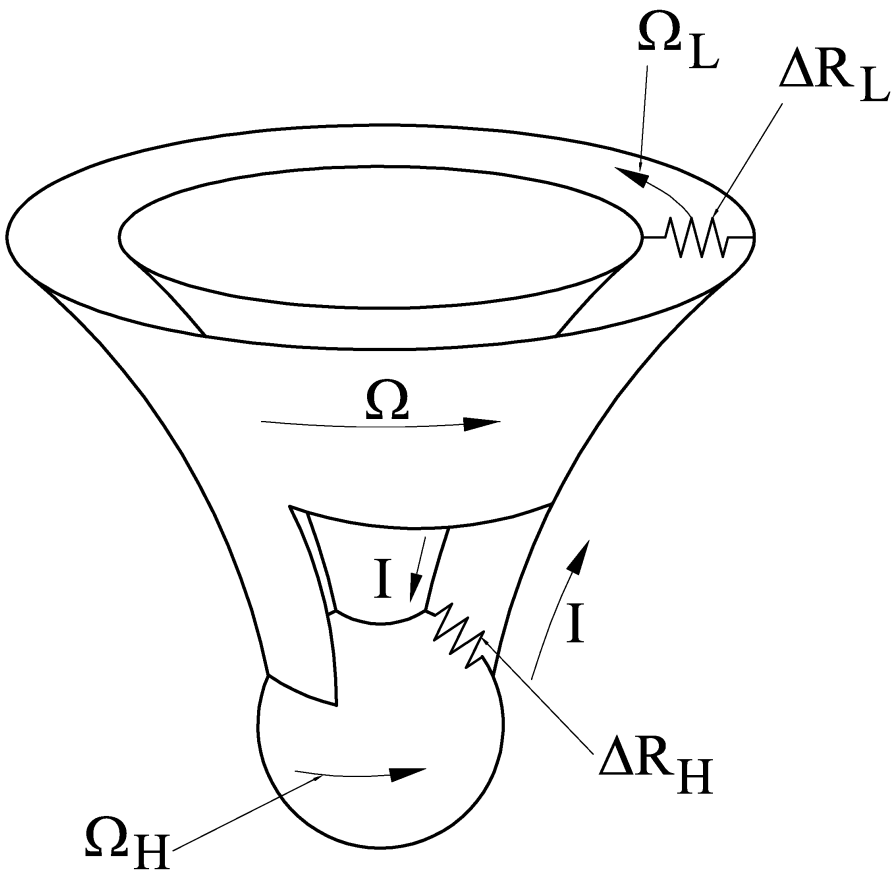

Figure: A circuit picture of the black hole spin energetics

Black hole Electrodynamics

$$\mathcal{I} = \int \mathbf{J}_H \cdot \mathbf{n} \mathrm{d}\ell = 2\pi J_H \varpi$$

$$\mathbf{E}_H = Z_0 \mathbf{J}_H = -\frac{1}{c}(\mathbf{v} \times \mathbf{B}) = -\frac{1}{c}(\Omega_F - \Omega_H)\nabla\psi$$

The luminosity through a ring at latitutde θ is given by

$$\Delta\mathcal{L} = \frac{\Omega_F(\Omega_H - \Omega_F)}{4\pi c}\varpi^2 B_n \Delta\psi,$$

where $\varpi(\theta) = R_H(j)\sin\theta$ is the ring radius, $\Omega_H(j)$ is the angular velocity of the hole, Ω_F is the angular velocity of the field, $B_n = \mathbf{B}\cdot\mathbf{n}$ is the field perpendicular to the hole surface and $\Delta\Psi(\theta)$ is the flux through a ring at θ of arc length $R_H(j)\Delta\theta$, which is given by

$$\Delta\psi(\theta) = 2\pi\varpi(\theta)R_H(j)B_n\Delta\theta.$$

The torque over the same ring is given by

$$\Delta\mathcal{G} = \frac{\Delta\mathcal{L}}{\Omega_H - \Omega_F}.$$

Black hole Electrodynamics

Now when the above equations for the power and torque are integrated over θ we obtain

$$\mathcal{L} = \frac{B_\perp^2 R_H(j)^4 \Omega_H(j)^2}{8c} g \quad \text{and}$$

$$\mathcal{G} = \frac{B_\perp^2 R_H(j)^4 \Omega_H(j)}{4c} f,$$

where the geometric factors factors f and g are found to be

$$\begin{aligned} f &= \int_0^\pi \left(\frac{(\mathbf{B}\cdot\mathbf{n})^2}{B_\perp^2}\right)\left(\frac{2\Omega_F}{\Omega_H}\right)\sin^3\theta\,\mathrm{d}\theta \\ g &= \int_0^\pi \left(\frac{(\mathbf{B}\cdot\mathbf{n})^2}{B_\perp^2}\right)\left(\frac{4\Omega_F}{\Omega_H}\right)\left(1-\frac{\Omega_F}{\Omega_H}\right)\sin^3\theta\,\mathrm{d}\theta, \end{aligned}$$

where $\mathbf{B}$ and Ω_F could be functions of θ and $B_\perp^2 \equiv \int_0^\pi (\mathbf{B}\cdot\mathbf{n})^2 \sin^3\theta\,\mathrm{d}\theta$ is the angle averaged root mean squared value of the normal component of the field on the surface of the hole.

Black hole Electrodynamics

These factors are of order unity; if the maximum power is transferred, then $\Omega_F = \Omega_H/2$, and both of these integrals are unity.
$R_H(j)$ and $\Omega_H(j)$, which are respectively the black hole's radius and angular velocity and are given by

$$\begin{aligned} R_H(j) &= r(j)m = \left(1 + (1-j^2)^{1/2}\right) GM_\bullet/c^2, \\ \Omega_H(j) &= \left(\frac{j}{2}\right) \frac{c}{R_H(j)}. \end{aligned}$$

Spin down time scale

The formulation of the BZ model in Macdonald & Thorne (1982) leads to the following forms for the jet power, $\mathcal{L}$ and torque, $\mathcal{G}$,

$$\mathcal{L} = \mathcal{L}_0 j^2 r^2(j) \text{ where } \mathcal{L}_0 = \frac{m^2 c}{32} B_\perp^2 g$$

$$\mathcal{G} = \mathcal{G}_0 j r^3(j) \text{ where } \mathcal{G}_0 = \frac{m^3}{8} B_\perp^2 f.$$

The angular momentum budget and the rotation energy budget are given by, respectively

$$\begin{aligned} \mathcal{J} &= \mathcal{J}_0 j \text{ where } \mathcal{J}_0 = c M_\bullet m \quad \text{and} \\ \mathcal{E} &= \mathcal{E}_0 \left(1 - \frac{r^{1/2}(j)}{\sqrt{2}}\right) \text{ where } \mathcal{E}_0 = M_\bullet c^2. \end{aligned}$$

Fiducial Values

We give the fiducial values of the various quantities

$$\begin{aligned}
\mathcal{J}_0 &= cM_\bullet m = 9\times10^{64} M_8^2 \ (\mathrm{g\ cm^2/s}) \\
\mathcal{L}_0 &= \frac{m^2 c}{32} B_\perp^2 g = 2\times10^{43} g B_4^2 M_8^2 \ (\mathrm{erg/s}) \\
\mathcal{G}_0 &= \frac{m^3}{8} B_\perp^2 f = 4\times10^{46} f B_4^2 M_8^3 \ (\mathrm{erg/s^2})
\end{aligned}$$

This lets us compute a spin-down time from angular momentum conservation

$$\tau_{j,BZ} = \frac{\mathcal{J}_0}{\mathcal{G}_0}\int_{j_f}^{j_i}\frac{\mathrm{d}j}{r^3(j)j} = 7.0\times10^8\ \mathrm{yrs}\ \frac{[(\kappa(j_i,j_f)/0.1)]}{B_4^2 M_9 f}$$

where, j_i and j_f are the initial and final spins, respectively, $\kappa(j_i,j_f)$ is the value of the integral, $B_4 = B/10^4$ Gauss and $M_9 = M_\bullet/10^9 M_\odot$.

Spin down time scale

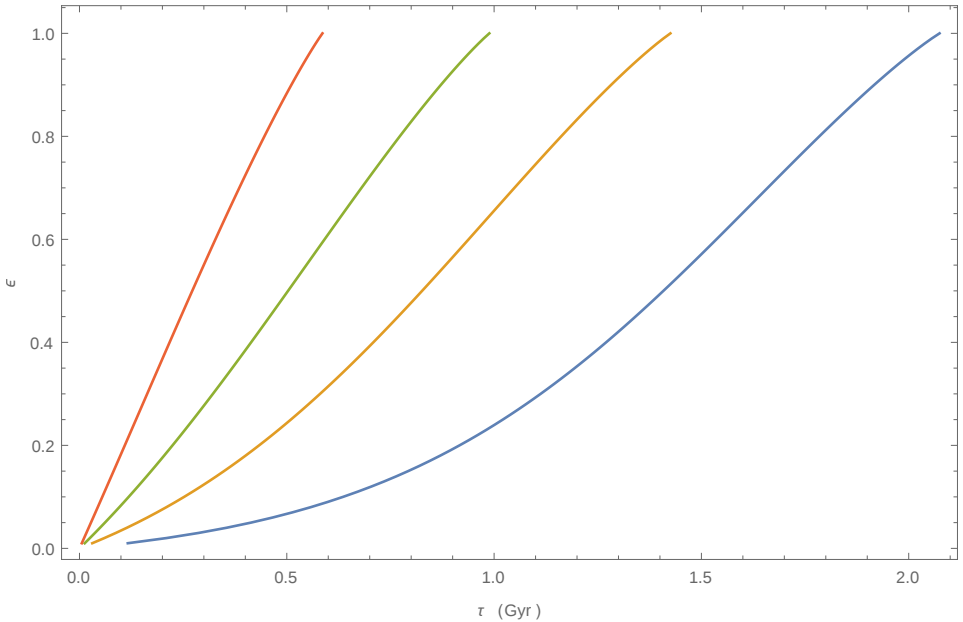

Figure: The fraction of BH rotational energy, ϵ, lost by the BZ process as a function of time is shown for various initial values of the BH spin parameter $j = 0.2, 0.4, 0.6, 0.8$ from right to left. The values assumed for other parameters are $B_4 = 1, M_9 = 1$.

Spin down time scale

We evaluate the energy radiated when the spin reduces from $j_i \rightarrow j_f$ to be

$$\Delta\mathcal{E} = \int \mathcal{L}\mathrm{d}t = \mathcal{L}_0 \int r^2(j) j^2 \left[\frac{\mathrm{d}j}{\mathrm{d}t}\right]^{-1} \mathrm{d}j$$

As a fraction of the rotational energy budget, this is found to be

$$\epsilon(j_i, j_f) \equiv \frac{\Delta\mathcal{E}}{\mathcal{E}} = \left[\int_{j_i}^{0} \frac{j}{r(j)}\mathrm{d}j\right]^{-1} \int_{j_i}^{j_f} \frac{j}{r(j)}\mathrm{d}j$$

The integral κ defined in Eqn (91) is calculated to be

$$\kappa(j_i, j_f) = \left[\left(\frac{1}{16}\right)\ln\left(\frac{2-w}{w}\right) + \left(\frac{3w^2+3w-4}{24w^3}\right)\right]_{w_f}^{w_i}$$

where $w_i = r(j_i)$ and $w_f = r(j_f)$. Using similar techniques the integral

$$\chi(j_i, j_f) \equiv \int_{j_i}^{j_f} \frac{j}{r(j)}\mathrm{d}j = \left[\ln(w) - w\right]_{w_i}^{w_f}.$$

The time to spin down is found to be 0.5 Gyr.

Spin down time scale

The $\mathcal{L}(j)$ goes through a maximum at $j = \sqrt{3}/2$. The evolution of the power as a function of time. The spin down time scale is likely to be reduced further when the mass of the hole increases by Bondi accretion (with negligible net angular momentum) as it spins down.

The effective timescale is estimated to be $\tau_{spin} \approx \frac{(\tau_a/2)\tau_j}{(\tau_j + \tau_a/2)}$, where the accretion time scale is $\tau_a \equiv \frac{M_\bullet c^2}{L_E}$ =0.45 Gyr, where L_E is the Eddington luminosity. As a result, $\tau_{spin} \approx 0.2$ Gyr for the typical case $j_i = 0.5, M_9 = 1, B_4 = 1$. Note that the timescales derived above are inversely proportional to the BH mass.

Spin down time scale: Mangalam et al. (2009)

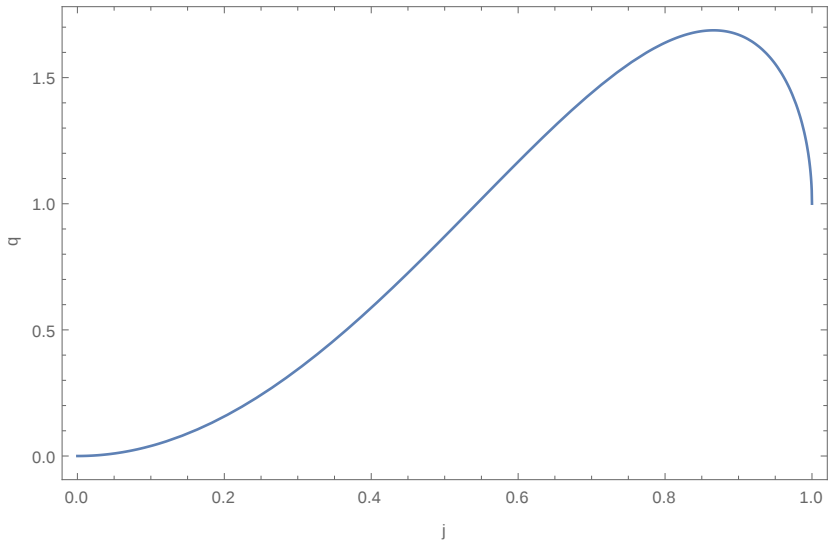

Figure: The power reduction factor, q, of the BZ jet as a function of the BH spin parameter j. The power goes through a maximum at $j = \sqrt{3}/2$ before dropping; this is due to the competition between the horizon radius and the spin of the hole.

Spin down time scale: Mangalam et al. (2009)

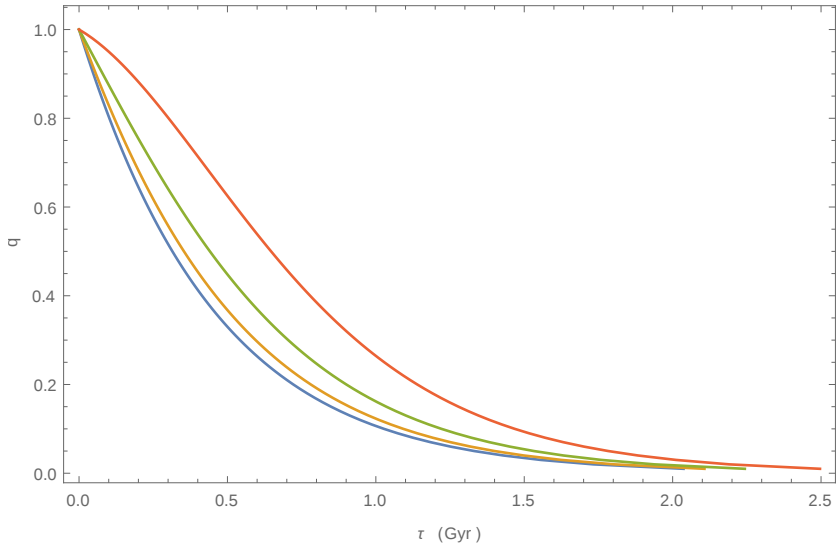

Figure: The power reduction factor, q, of the BZ jet as a function of time is shown for various initial values of the BH spin parameter $j = 0.2, 0.4, 0.6, 0.8$ from bottom to top. The values assumed for other parameters are $B_4 = 1, M_9 = 1$.

Energy loss time scale

The energy loss time-scale is quite similar for the hybrid model, although the dependence on BH mass is much more gradual. For the Meier (1999) model we find the time scale

$$\tau_{L,hybrid} = 5 \times 10^8 \mathrm{yr}\ \alpha_{-2}^{-1/10} M_9^{-1/10} \dot{m}_{-3}^{-4/5} \zeta_{-1}^{-1},$$

Black Hole Mass and Spin Evolution: Mangalam (2015)

$$\epsilon_M \equiv L/\dot{M}_0 c^2,$$

where $\dot{M}_0$ is the rate of rest-mass accretion and L is the luminosity. Define ϵ_L, the efficiency of accretion luminosity, according to

$$\epsilon_L \equiv L/L_E,$$

where L_E is the Eddington luminosity, given by

$$L_E = \frac{4\pi M_\bullet \mu_e m_p c}{\sigma_T} \approx 1.3 \times 10^{46} \mu_e M_8 \text{ erg s}^{-1}.$$

$$\frac{dM_\bullet}{dt} = (1 - \epsilon_M)\dot{M}_0.$$

Black Hole Mass and Spin Evolution

Combining we obtain the black hole growth rate,

$$\frac{\mathrm{d}M_\bullet}{\mathrm{d}t} = \frac{\epsilon_L(1-\epsilon_M)}{\epsilon_M}\frac{M_\bullet}{\tau_a},$$

where τ is the characteristic accretion timescale,

$$\tau_a \equiv \frac{M_\bullet c^2}{L_E} \approx 0.45\mu_e^{-1}\ \mathrm{Gyr},$$

and is independent of $M_\bullet$.
The mass accretion efficiency ϵ_M is typically a function of the black hole spin parameter $j = J/M^2$.

$$\frac{\mathrm{d}j}{\mathrm{d}t} = \frac{\epsilon_L}{\epsilon_M}\frac{j}{\tau} \quad + \mathrm{BZ\ \ TORQUE}$$

In general, eqns must be integrated simultaneously to determine the mass and spin evolution of the black hole.

Bondi Case

This is the case where net spin content in the accreting material is zero but the mass increases the horizon radius which reduces the spin.

$$\dot{\mathcal{J}} = \mathcal{J}_0 \dot{j} + 2\frac{\mathcal{J}_0}{M_\bullet}\dot{M}_\bullet j$$

which should be matched to the BZ torque. This results in the following equation for the spin parameter

$$-\left[\frac{2\epsilon_L(1-\epsilon_M)}{\epsilon_M \tau_a} + \frac{\mathcal{G}_0}{\mathcal{J}_0} r(j)^3\right] j = \frac{\mathrm{d}j}{\mathrm{d}t}.$$

We write $\mathcal{G}_0/\mathcal{J}_0 = \mu/\tau_j$, where $\mu = M_\bullet/M_s$. So we find the coupled set of differential equations for the mass and spin:

$$\begin{aligned} \frac{\mathrm{d}j}{\mathrm{d}t} &= -\left[\frac{2\epsilon_L(1-\epsilon_M)}{\epsilon_M \tau_a} + \frac{\mu}{\tau_j} r(j)^3\right] j \\ \frac{\mathrm{d}\mu}{\mathrm{d}t} &= \frac{\epsilon_L(1-\epsilon_M)}{\epsilon_M}\frac{\mu}{\tau_a} \end{aligned} \tag{63}$$

Bondi Case

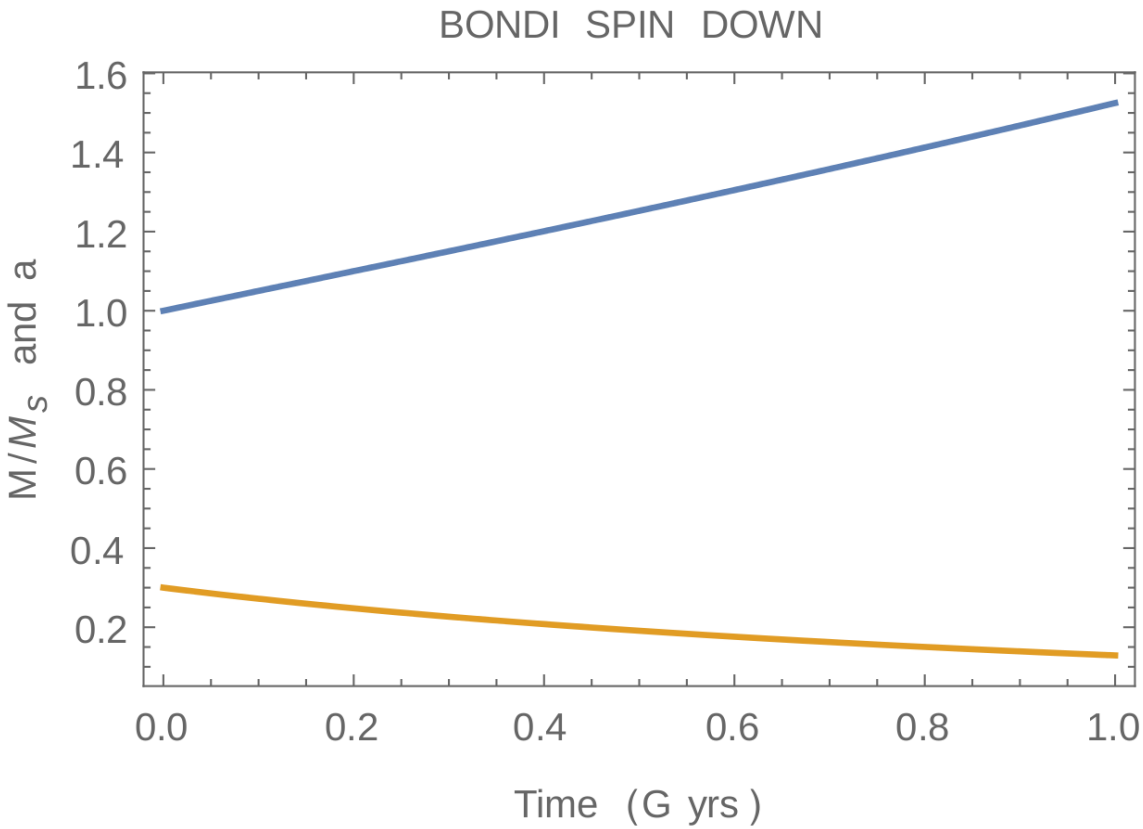

Figure: An illustration of Bondi spin down for seed mass of $M_8 = 0.01$ for inital $a = 0.3$

Thin disk Case

In a standard thin disk corotating with the black hole, the energy and angular momentum per unit rest mass accreted by a black hole are the energy and angular momentum of a unit mass at the ISCO, immediately prior to its rapid plunge and capture by the hole:

$$\tilde{E}_{\rm ISCO} = \frac{r_{\rm ms}^2 - 2Mr_{\rm ms} + a\sqrt{Mr_{\rm ms}}}{r_{ms}(r_{ms}^2 - 3M_h r_{ms} + 2a\sqrt{Mr_{ms}})^{1/2}}$$

$$\tilde{l}_{\rm ISCO} = \frac{\sqrt{Mr_{\rm ms}}(r_{\rm ms}^2 - 2a\sqrt{Mr_{\rm ms}} + a^2)}{r_{ms}(r_{ms}^2 - 3M_h r_{ms} + 2a\sqrt{Mr_{ms}})^{1/2}},$$

where the ISCO radius $r_{\rm ms}$ is given by

$$r_{\rm ms} = M\{3 + Z_2 - [(3 - Z_1)(3 + Z_1 + 2Z_2)]^{1/2}\},$$

$$Z_1 \equiv 1 + \left(1 - \frac{a^2}{M^2}\right)^{1/3}\left[\left(1 + \frac{a}{M}\right)^{1/3} + \left(1 - \frac{a}{M}\right)^{1/3}\right],$$

$$Z_2 \equiv \left(3\frac{a^2}{M^2} + Z_1^2\right)^{1/2}$$

Thin disk Case

The mass accretion efficiency and spin evolution parameters corresponding to the thin disk model are then given by

$$\epsilon_M = 1 - \tilde{E}_{\rm ISCO},$$

$$\frac{{\rm d}j}{{\rm d}t} = \left(\tilde{l}_{\rm ISCO} - 2\frac{a}{M}\tilde{E}_{\rm ISCO}\right)\frac{\epsilon_L}{\epsilon_M(j)\tau_a} \quad \text{(standard thin disk)}.$$

This leads to the following coupled differential equations

$$\begin{aligned}
\frac{{\rm d}j}{{\rm d}t} &= \frac{\tilde{l}_{\rm ISCO}\epsilon_L}{\epsilon_M(j)\tau_a} - \left[\frac{2\epsilon_L(1-\epsilon_M)}{\epsilon_M\tau_a} + \frac{\mu}{\tau_j}r(j)^3\right]j \\
\frac{{\rm d}\mu}{{\rm d}t} &= \frac{\epsilon_L(1-\epsilon_M)}{\epsilon_M}\frac{\mu}{\tau_a}
\end{aligned}$$

Thin disk Case

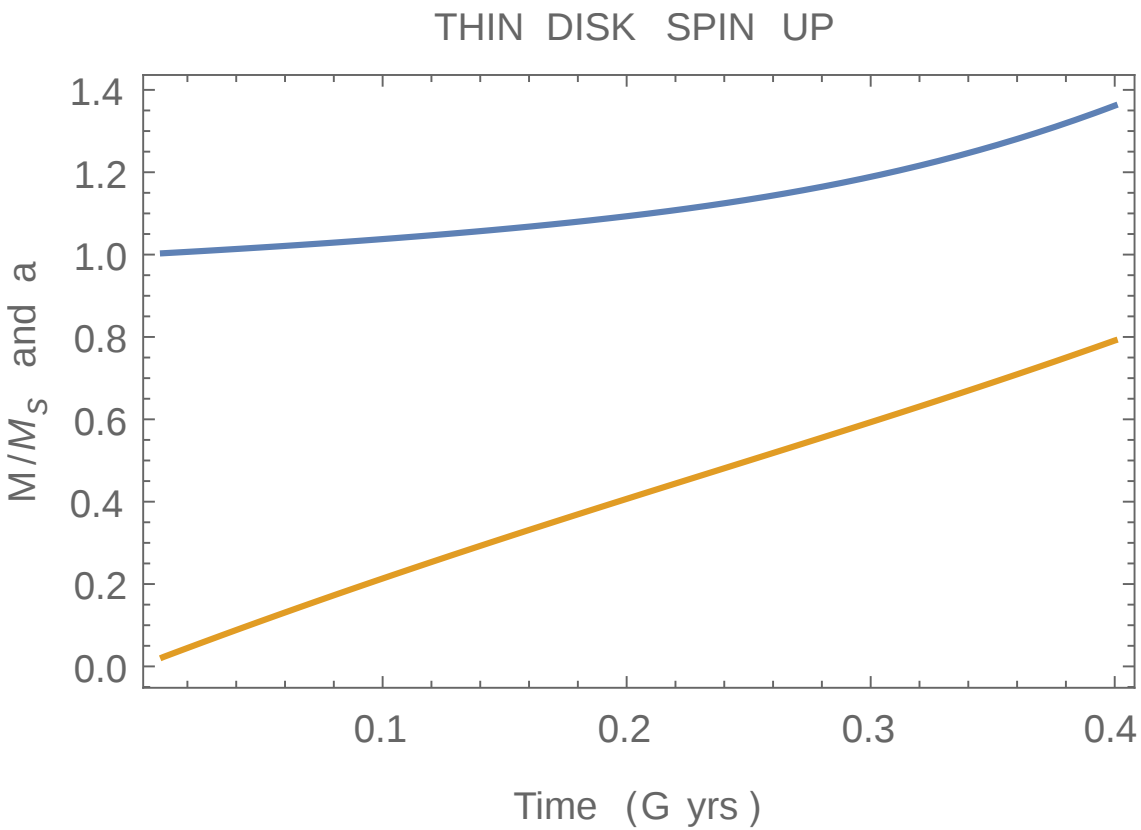

Figure: An illustration of Bondi spin down for seed mass of $M_8 = 0.01$

MHD disk Case

The MHD disk accretion model of Gammie, Shapiro & McKinney (2004) and McKinney & Gammie (2004) is based on a fully relativistic, axisymmetric simulation of a nonradiative, magnetized plasma onto a Kerr-Schild black hole within the MHD approximation.
The results of the numerical simulations suggest that can be represented reasonably well by the least squares linear fit

$$\tilde{l}_{\rm ISCO} - 2\frac{a}{M}\tilde{E}_{\rm ISCO} = 3.14 - 3.30\frac{a}{M} \quad ({\rm MHD\ disk}),$$

The numerical simulations demonstrate that the above parameters describing steady-state, MHD accretion-disk behavior are not particularly sensitive to the initial conditions in the disk (e.g. the initial $B-$field). The key results are also quite comparable to those found by De Villiers et al. (2004), who used a different numerical method and took the adiabatic index of the gas to be $\Gamma = 5/3$ instead of $\Gamma = 4/3$. We therefore model a relativistic MHD accretion disk in our evolution equations.

MHD disk Case

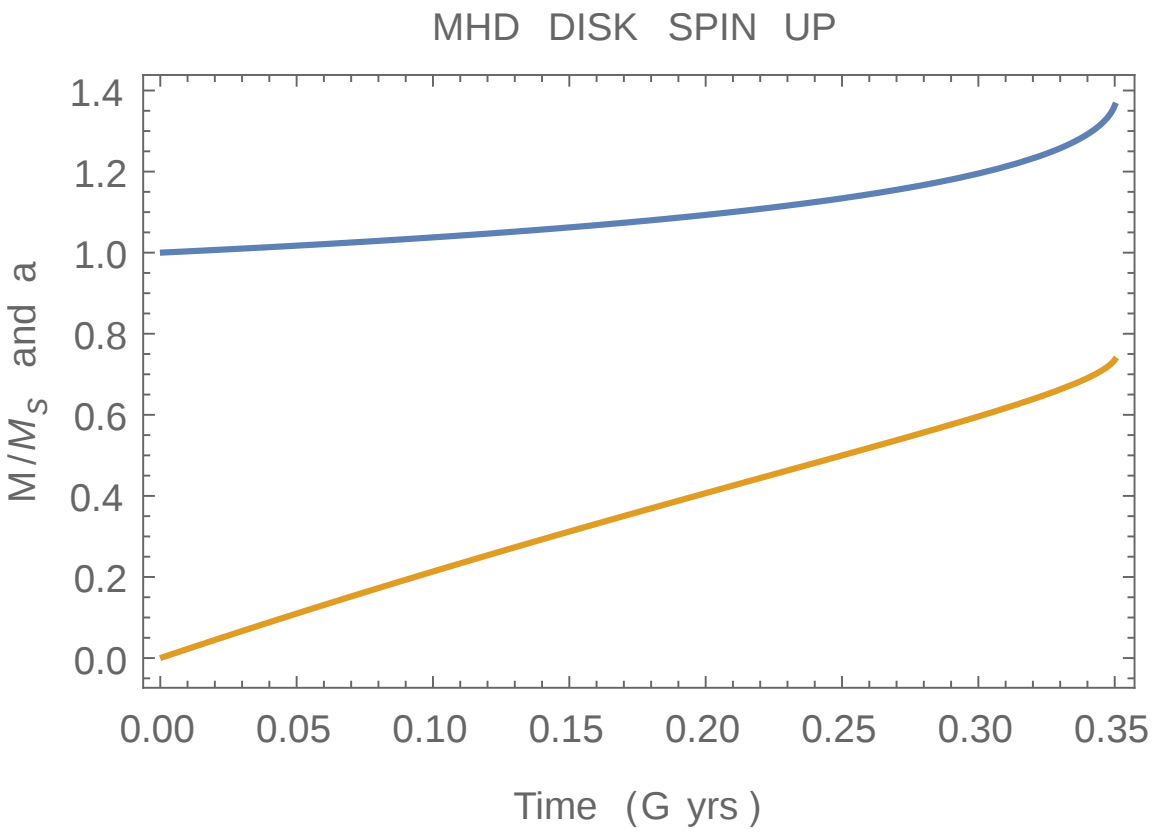

Figure: An illustration of Bondi spin down for seed mass of $M_8 = 0.01$

Conclusions

- We have focused largely on the Blandford-Znajek mechanism of extracting rotational energy from the BH. In the absence of accretion torque. two time scales are derived using energy loss and power reduction as criteria for determining the spin (*Mangalam et al. 2009, MNRAS, 397, 2216*).
- The spin-down time scale for the case of no accretion is about $\tau_{spin} = 0.5/(B_4^2 M_9)$ Gyr. The evolution of the jet power indicates an increase before a gradual decline if the initial spin, $j > \sqrt{3}/2$, as a result of the hole's increasing size. This naturally has implications for the evolution of the jet.
- When the Bondi accretion is on, $\tau_{spin} \approx \dfrac{(\tau_a/2)\tau_j}{(\tau_j + \tau_a/2)}$, where the accretion time scale is $\tau_a \equiv \dfrac{M_\bullet c^2}{L_E}$ =0.45 Gyr, resulting in a spin down time scale of 0.3 Gyr.

Model parameters $M_\bullet, L, L_j, j, \dot{M}_\bullet, z$

Conclusions

- When there is thin disk with MHD accretion then $\tau_{spin} \approx \frac{(\tau_a \theta)\tau_j}{(|\tau_j - \tau_a \theta|)}$, then the *spin up* time scale is typically 0.35 Gyr.
- An important issue is the maximum spin j that can be achieved in disk accretion process. Preliminary results indicate that the black hole acheives about 98% of the maximum value ($j_{max} = 0.998$, Thorne 1974) when there is no jet and 93% of j_{max} when there is a jet. This is model dependent and in reasonable agreement with various simulations; eg. Benson & Babul (2009).
- It is planned to expand this work to hybrid models in greater detail, and to thus explore other discs in ADAF mode.
- The results have natural implications to the black hole demographics with parameters:
  $M_\bullet, z, L_{jet}(j), L(M_\bullet)$
  and one can model the cosmological evolution heuristically.

Open Questions

- How are the magnetic fields generated?
- What is the physics of the $M - \sigma$ relationship?
- What is the stellar feeding rate of black holes?
- How do the black holes form?